ABSTRACT

Title of dissertation:	MORPHOLOGICAL CLUES TO THE XRAY EMISSION FROM POWERFUL EXTRAGALATIC JETS
	Karthik Reddy Solipuram, Doctor of Philosophy, 2022
Dissertation directed by:	Dr. Markos Georganopoulos Dr. Eileen T. Meyer Department of Physics

MORPHOLOGICAL CLUES TO THE XRAY EMISSION FROM POWERFUL EXTRAGALACTIC JETS

by

Karthik Reddy Solipuram

Dissertation submitted to the Faculty of the Graduate School of the
University of Maryland, Baltimore County in partial fulfillment
of the requirements for the degree of
Doctor of Philosophy
2022

Advisory Committee:
Dr. Markos Georganopoulos, Chair/Advisor
Dr. Eileen T Meyer, Co-Advisor/Reader
Dr. Zhibo Zhang
Dr. Aneta Siemiginowska
Dr. Bradford Snios, Reader

Preface

If needed.

Foreword

If needed.

Dedication

If needed.

Acknowledgments

Table of Contents

List of Figures vii

List of Abbreviations viii

1 Introduction 1
- 1.1 Extragalactic Astronomy: The beginning 1
- 1.2 Active Galactic Nuclei: A new paradigm 3
  - 1.2.1 Radio Astronomy 4
  - 1.2.2 Discovery of Quasars 6
  - 1.2.3 Discovery of Relativistic Jets from AGN 7
- 1.3 Radiative processes 10
  - 1.3.1 Synchrotron Radiation 10
  - 1.3.2 Inverse Compton Radiation 14
  - 1.3.3 Relativistic effects 15
- 1.4 Active Galactic Nuclei: The current model 18
  - 1.4.1 AGN Taxonomy 19
    - 1.4.1.1 Jetted AGN 20
    - 1.4.1.2 Non-jetted AGN 23
  - 1.4.2 The Central Engine 24
    - 1.4.2.1 Detecting SMBH in AGN 24
    - 1.4.2.2 Disk Accretion and the Eddington Limit 26
    - 1.4.2.3 Jet launching 27
- 1.5 X-ray jets 30
  - 1.5.1 The Chandra X-ray Observatory 31
  - 1.5.2 The IC/CMB model 32
  - 1.5.3 Issues with the IC/CMB model 34
  - 1.5.4 Modified IC/CMB and Alternatives 37
  - 1.5.5 Knot and Offset Formation 39
- 1.6 This Thesis 42

List of Figures

1.1 A VLA 8.4GHz radio image of the relativistic jet in M87 8
1.2 A simplified schema of the current model of the AGN, not drawn to scale. The taxonomy of the AGN is a result of the presence or absence of various components and observational effects. Figure reproduced from Beckmann and Shrader (2012). 18
1.3 Typical example images for the FR I and II classes. (a) shows a VLA radio image of an FR-I source, M84, where the where the jet's brightness gradually decreases with increasing distance from the core (image taken from DRAGN website, http://www.jb.man.ac.uk/atlas/). (b) shows a a radio image of an FR-II source, Cygnus A. Two jets originate from the core and terminate in bright hotspots, feeding accelerated plasma into the radio lobes (image taken from NED, http://ned.ipac.caltech.edu). 21
1.4 The X-ray and radio images of PKS0637-752, the first detection of an X-ray jet by *Chandra*. Image taken from Chartas et al. (2000) . . 32
1.5 (a) The spectrum of knot W7.8 of PKS0637-752 where the solid line is the synchrotron component. Under equipartition condition, the dashed line indicates the SSC component while the dotted line, the inverse-Compton component from a non-relativistic jet, and both the mechanisms fail to account for the observed X-ray emission. Image taken from Chartas et al. (2000) (b) The Spectral energy distribution (SED) of knot W7.8 of PKS 0637-752. The X-ray emission can be explained by IC/CMB if the jet is closely aligned and highly relativistic, and the up-scattering electrons have low energies (much lower than what is traced by the radio-optical spectrum). Image taken from Tavecchio et al. (2000). 33
1.6 A smoothed X-ray image of 3C111, overlaid with the VLA 8.4 GHz radio contours. The X-rays peak and decay before the radio in multiple knots including K9, K30, K45, K61, which appear as peak to peak offsets. Image taken from Clautice et al. (2016) 37

List of Abbreviations

Γ	bulk Lorentz factor
γ	Lorentz factor
NED	NASA Extragalactic Database
VLA	Very Large Array
ATCA	Australia Telescope Compact Array
JVLA	Karl G. Jansky Very Large Array
IC	Inverse Compton
CMB	Cosmic Microwave Background
LIRA	Low Count Image Reconstruction and Analysis

Chapter 1: Introduction

1.1 Extragalactic Astronomy: The beginning

Nebulae, which stand for clouds in Latin, have been an integral part of astronomy since the Middle Ages and were one of the main driving forces behind extragalactic hypotheses. Their first known record dates back to 150 AD, who recorded five objects in the sky as “nebulous” in his books VII-VIII of *Almagest*. Abd al-Rahman al-Sufi noted a “little cloud” during 964 AD in his work *Book of fixed Stars*, which we now know as the Andromeda Galaxy. On July 4th, 1054, Chinese and Persian astronomers have recorded the supernova event of the Crab nebula.

With the advent of refracting telescopes, mainly built based on the designs developed by Hans Lippershey in the early 17th century, Orion nebula has been detected and studied in detail by French and Swiss astronomers. Several more nebulae have been cataloged by the middle of the 18th century. In 1715, Edmund Halley published a list of six, Jean-Philippe de Cheseaux twenty with eight newer ones in 1745, Nicolas Louis de Lacaille 42 between 1751-1753. Later in 1781, Charles Messier compiled a list of 103, which are now called Messier objects, including the famous M87.

The number of known objects substantially improved with the works of William Herschel and his sister Caroline who published catalogs with more than a thousand nebulae during the 1780s. However, it was unclear at the time whether some of these objects were located outside the Milky Way. Based on the work of Wright (1750), who explained the Milky Way as a humungous spinning disk with several layers of stars, Kant (1755) hypothesized that some nebulae with a fuzzy spiral shape might be independent Milky Ways themselves and termed them "island universes". He also suggested the others were thin gas and dust clouds within the Milky Way, collapsed into a spinning disk forming stars and planets, commonly called the nebular hypothesis–both commonly interpreting nebulae as collections of stars. Herschel (1785) later noted a reddish region in the central regions of Andromeda, which did not appear anything like a star or known gaseous nebulae, advancing Kant's extragalactic hypothesis. These results resulted in an intense debate in the community. Many astronomers sided with Laplace, who maintained the nebular hypothesis view for spiral nebulae, while a few believed in the extragalactic origin.

Huggins (1864) noted that the spectra of Andromeda resemble a continuum overlaid with absorption lines and concluded that they were stellar in nature. Fath (1909) found similar spectra in a few more nebulae. Interestingly some emission lines from one nebula, NGC 1068, were found to have a width of $\sim$3000 km/s, similar to the lines found in nearby gaseous nebulae, supporting both the hypotheses. Later Slipher (1913) noted that the lines from Andromeda display a redshift higher than the escape speed of Milky Way, thereby indicating an extragalactic origin. These conflicting views sparked the "Great Debate" in astronomy (Shapley and Curtis,

1921) between Harlow Shapley and Heber Curtis in April 1920, each favoring the nebular and extragalactic views, respectively, based on different arguments. For example, Shapley argued that the energy output of the nova observed in Andromeda (Backhouse, 1888) would be physically impossible to explain if it were an external galaxy. Conversely, Curtis showed that the nova events in Andromeda outnumbered those in Milky Way and questioned why the events must be disproportionately large in a specific region of the Milky Way if Andromeda were to be a part of it.

Later, Opik (1922) estimated the distance of Andromeda to be about 450 kpc (which is half the actual value), placing it well outside our Galaxy. The debate was finally settled in the late 1920s by Hubble (1929) who used Cephid variables to confirm Andromeda's extragalactic origin. Cephids are stars with a cycle of brightness whose frequency correlates with their luminosity, allowing us to determine their distance.

1.2 Active Galactic Nuclei: A new paradigm

Although Hubble's work validated the presence of extragalactic objects, the nature of the bright emission lines from centers some galaxies, however, remained unknown for a decade or two. Seyfert (1943) obtained the spectra of six galaxies and found that they show high-excitation emission lines superimposed on a solar-like continuum with widths reaching up to 8500 km/s. These types of galaxies are now called as *Seyfert Galaxies*. Woltjer (1960) noted that parsec scale emission from these galaxies requires a mass of $\sim 10^8$ solar masses ($M_\odot$). Fowler and Hoyle (1963) made an important advance by suggesting that the centers of these galaxies host a massive star; they would emit by accreting dust from the surroundings. A year later, another idea emerged, which assumed that the central object is a black hole rather than a massive star (Salpeter, 1964; Zel'dovich and Novikov, 1964). Such galaxies, whose bright centers are powered by accretion onto a black hole, are what we now call Active Galactic Nuclei (AGN). AGN are the most luminous and steady sources of luminosity in the universe. They have a broad spectrum covering 20 orders of magnitude in frequency, and their luminosity ranges from $10^{40} - 10^{49}$ ergs s^{-1} and are one of the most actively studied classes of objects in astronomy.

1.2.1 Radio Astronomy

Radio astronomy also provided essential contributions to our understanding of AGN. Its history dates back to the early 1930s. In 1932, Karl Guthe Jansky, an engineer at Bell Labs, noted that a radio signal peaked with a period of 24hrs and suspected that they were radio waves from the Sun. Upon gathering more data, he found that the signal repeated with the frequency of a Sidereal day: the time it takes for distant stars to rotate once in our field of view. These findings eventually led Jansky to conclude that the signal came from the central regions of our galaxy (Jansky, 1932), and it marked the first serendipitous discovery of an astronomical radio source and the birth of radio astronomy. He was honored for his seminal contributions to this field by naming the units of flux as Jansky (Jy) after his name.

Inspired by this discovery, Grote Reber, an amateur radio engineer, built a parabolic radio telescope in his backyard with a 9m diameter. He mapped the emission from the galactic center at 160 MHz and not only confirmed Jansky's discovery (Reber, 1940) but also showed that the emission exhibits a non-thermal spectrum. Although World War II intervened during this period and hindered research in astronomy, it led to advances in radar technology and, consequently, in radio astronomy.

Martin Ryle and Antony Hewish developed Earth-rotation aperture synthesis techniques in the 1950s, allowing emulation of a large aperture-telescope using a network of several spatially-separated smaller telescopes called baselines. With the arrival of efficient computing machines capable of performing the required inverse Fourier transforms, it was possible to build radio telescopes with one mile and later with 5 km apertures. These telescopes were used to conduct the 3C and 3CR sky-surveys at 159 MHz and 178 MHz, respectively, detecting several hundreds of radio sources (Bennett and Simth, 1962; Edge et al., 1959) including well-known sources like 3C 48 and 3C 273. While some had extremely faint star-like optical detections showing emission lines matching with no known element on earth at that time (Matthews and Sandage, 1963), the low resolution of these surveys precluded accurate identification of optical counterparts for many of them. Their optical variability ruled out a normal galaxy-like origin, and their extreme brightnesses prevented a stellar interpretation, leading astronomers to call such sources as *quasi-stellar (star-like) sources*, shortened to *quasar* (Chiu, 1964).

1.2.2 Discovery of Quasars

A few years later, measurements of 3C 273 based on lunar-occultation technique allowed Schmidt (1963) to identify its optical counterpart with a magnitude of 13, again showing unknown lines; it also contained a structure he referred to as "a faint wisp or jet." They both lay close to the radio positions of two bright components in 3C 273. The optical spectrum of 3C 273 exhibited a complex continuum with broad emission lines (Oke, 1963). Schmidt (1963) showed that the emission lines from 3C 273 match Balmer and Mg II lines at a redshift of $z = 0.158$. Furthermore, (Oke, 1963) found that a previously unidentified line in the infrared matched with an Hα line with this redshift. A similar interpretation led to determining the redshift of 3C 48 as 0.37. These redshifts implied an extragalactic origin and a higher than typical luminosity.

After Salpeter (1964) and Zel'dovich and Novikov (1964) advanced the idea of a black hole at the center of an AGN, Lynden-Bell (1969) put forward an idea that accretion onto black holes with sufficient mass can power the high luminosity of quasars. He also argued that it could produce the observed thermal continuum and broad emission lines and be the process behind quasars and Seyfert galaxies. This idea was rapidly accepted by the community, marking the dawn of the basic AGN paradigm. Astronomers now widely believe that practically all the galaxies host a supermassive black hole (SMBH) at their center (e.g., Richstone et al., 1998), powering AGN via accretion. The Event Horizon Telescope provided direct evidence for the existence of an SMBH by imaging its silhouette in M87 (Event Horizon

Telescope Collaboration et al., 2019).

1.2.3 Discovery of Relativistic Jets from AGN

In the late 1960s, Hogg et al. (1969) detected extended radio emission from M87, which was previously identified as a “curious straight ray” by Curtis (1918), coinciding with its extended optical component. Soon high-resolution sky-surveys conducted by radio interferometers at Cambridge revealed extended emission from several new extended sources (e.g., Northover, 1973; Turland, 1975) with the majority showing two-sided jets while one-sided from quasars. Moreover, these structures spanned a wide range of radio powers, however, it remained uncertain what determined their presence or absence and the sidedness. It was with the commissioning of the Very Large Array (VLA) with an unprecedented sensitivity and angular resolution, several *jets* could be delineated from diffuse radio structures (e.g., Bridle and Perley, 1984). In the mid 1960s, discoveries of optical variability and detection of several unresolved radio sources with growing baselines indicated the presence of small scale structures in some radio sources. This triggered the development of Very Long Baseline Interferometry (VLBI), a technique which is capable of detecting structures much smaller than the VLA, leading to the first detection of an apparent superluminal (or faster than light) motion (Cohen et al., 1971; Whitney et al., 1971), implying relativistic speeds. Several similar detections followed, and it began to be established that the observed extended morphologies are manifestations of relativistic jets from AGN (Blandford and Königl, 1979; Konigl, 1980), which from

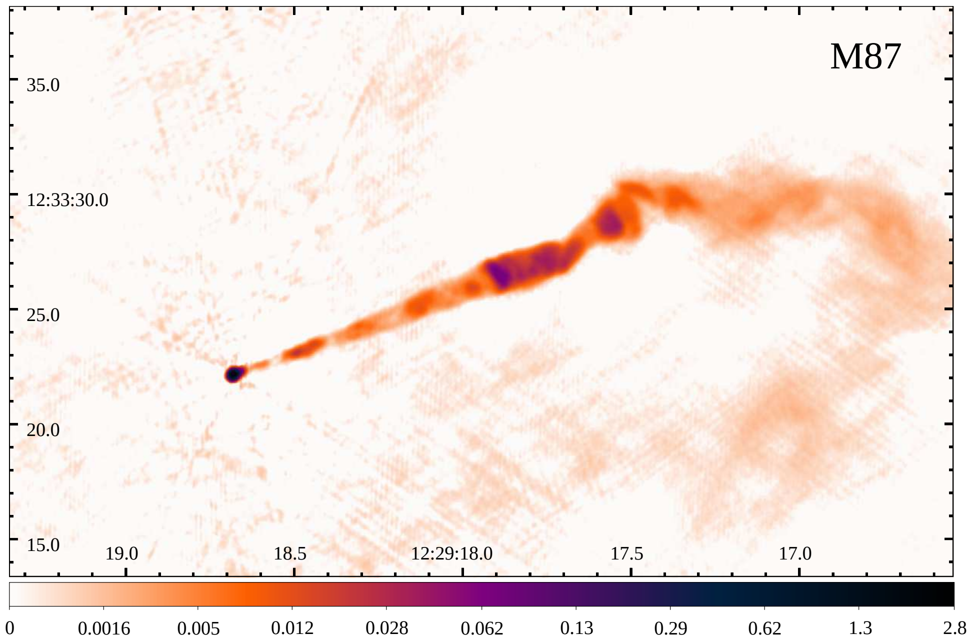

Figure 1.1: A VLA 8.4GHz radio image of the relativistic jet in M87

the broad subjects of my thesis. As an example, I show a VLA 8.4 GHz radio image of the one-sided jet in M87 in Fig. 1.1 at 0.2″ resolution. Despite the actual presence of twin jets in this source, due to a phenomenon called *Doppler Boosting*, which I discuss in section 1.3.3, the emission from the approaching jet is amplified, while it is diminished for the receding jet, making it undetectable.

While a few millions of AGN are detected so far (e.g., Assef et al., 2018), only a small fraction of them produce radio jets (e.g., Ivezić et al., 2002; Padovani, 2017). They transport energy and momentum from the central sub-parsec scale regions of the AGN out to parsec scales and often to kilo-parsec (kpc) and Mpc scales, with the largest known jet reaching a size of 5 Mpc (Oei et al., 2022), which is roughly 1/3rd of the distance between M87 and the Earth. Such jetted AGN are generally classified as 'radio-loud' AGN. Although the exact jet launching mechanism is unknown, it is commonly believed that a strong magnetization of the accretion disk coupled with the black hole's spin may produce outflows at relativistic speeds (Blandford et al., 2019).

The kinetic and radiative power output from these jets can stimulate and limit the growth of galaxies. It can also be responsible for producing high energy cosmic rays and intergalactic magnetic fields (for a recent review, see Blandford et al., 2019). It is plausible that the jets may have regulated black hole masses of the early universe (Churazov et al., 2005) via feedback. There is also growing evidence that jets may have shaped the baryonic (i.e., protons, neutrons, and alike) part of the local universe (Fabian, 2012). If so, the jets have profound implications for the universe's evolution.

Despite the significant role that jets may have played in galaxy evolution, we only know a little about jet physics even after studying them for more than half a century. For example, their particle composition–electrons and positrons or electrons and protons—is uncertain, as is the speed of the jets on kpc to Mpc scales. It is also unclear how jets remain collimated across large distance. Importantly, for the present work, how powerful jets emit X-rays hundreds of kpc away from the central AGN is unclear: two of the main competing models, which I describe in the final section of this chapter, imply orders of magnitude differences in the total power jets feed into their host galaxies and clusters. My thesis attempts to elucidate the properties of X-ray emission from such large scale jets.

In the following section, I introduce the radiative processes appropriate for the study of jets and then discuss the current model of AGN. I then discuss its resulting taxonomy and models proposed to explain the observed properties of jets. I then provide a detailed description of the current state of X-ray emission from large scale jets, the main subject of my thesis.

1.3 Radiative processes

The emission from large scale jets spans a wide spectrum ranging from radio to X-rays (e.g., Harris and Krawczynski, 2002; Worrall, 2009) and sometimes up to γ-rays (e.g., H. E. S. S. Collaboration et al., 2020; Meyer et al., 2019). The synchrotron mechanism has been successful in explaining the observed radio-to-optical spectra of all the jets and X-ray emission for most low-power jets (e.g., Hardcastle et al., 2001; **?**). Inverse Compton (IC) scattering is another form of raditation that is regularly invoked in the context of large scale jets. Although several other mechanisms have been proposed, for example, magnetic reconnection, their applicability for X-ray emission for large scale is still unclear. Hence, I restrict my discussion to synchrotron and IC mechanisms in the following sections.

1.3.1 Synchrotron Radiation

One of the most important characteristics of synchrotron radiation is a high degree (upto $\sim$70%) of polarization. This characteristic led to the first-ever proof that synchrotron radiation produces optical emission from the jet of M87 (Baade, 1956), and also quickly explained the radio emission from other jets.

Charged particles, when accelerated, emit electromagnetic radiation (for a review, see Longair, 2011). If the charged particles are relativistic and are accelerated by a magnetic field, they produce synchrotron radiation. The power radiated by a charged particle (mass=m and charge= Z) moving with a speed v in a magnetic field B, is proportional to

$$P_{synch} \propto \frac{Z^4 \gamma^2 B^2 v^2 \sin^2 \theta}{m^2} \tag{1.1}$$

where γ is the Lorentz factor and θ is the pitch angle. Because $P_{synch} \propto m^{-2}$, the emission is extremely efficient for electrons and positrons when compared to protons that are ~2000 times heavier. For an electron and proton travelling with the same speed, the power radiated by a proton will be smaller by a factor of 3×10^{-7} compared to an electron. That means, for a given synchrotron luminosity, a jet with radiating protons would demand a significantly higher energy budget than an electron-jet. Because of this radiative efficiency, only electrons (or positrons) are generally assumed to be emitting in jets for the purpose of radiative calculations.

The average power radiated by an electron for an isotropic distribution of pitch angles is given by

$$\langle P_{synch} \rangle = \frac{4}{3} \sigma_T \beta^2 \gamma^2 c U_B \tag{1.2}$$

where σ_T is the Thomson scattering cross-section, c is the speed of light, $\beta = v/c$ and $U_B = B^2/8\pi$ is the magnetic field energy density, and $\gamma = 1/\sqrt{1-\beta^2}$ is the Lorentz factor. Furthermore, the specific luminosity of a single electron spectrum peaks at $0.29\nu_{crit}$, where ν_{crit} is the critical frequency given by:

$$\nu_c = \frac{3\gamma^2 eB}{4\pi m_e c} \sin \theta \tag{1.3}$$

where e is the electron charge. That means, to produce synchrotron radiation at $\nu \sim 1$ GHz in a magnetic field of $B \sim 10^{-6}$ G, an electron requires $\gamma \sim 10^4$. Such extremely relativistic electrons in a jet can only be produced by an efficient particle acceleration mechanism, such as the first-order Fermi acceleration (Fermi, 1949).

The radio spectrum of a jet usually takes a powerlaw form $F_\nu \propto \nu^{-\alpha}$ where F_ν is the flux density, ν is the frequency, and α is the spectral index. I will use this definition for spectral index for the rest of my thesis. Lower α indicates a harder/flatter spectrum, while higher α indicates a softer/steeper spectrum. For a group of synchrotron emitting electrons in a jet, the resulting spectrum is a superposition of the individual spectra of the electrons. If the electron energies follow a powerlaw distribution, $n(E)dE = E^{-s}dE$ (where $n(E)dE$ in the number density of electrons in the energy range E to $E + dE$), the final spectrum is also a powerlaw given by $F_\nu \propto \nu^{-\alpha}$, where $\alpha = (s - 1)/2$.

In general, astrophysical sources display $\alpha \approx 0.75$ at $\nu \approx 1$ GHz implying that $s \approx 2.5$. The value of s indicates the index at which the electrons are originally injected in to the jet possibly via shocks and gets modified by synchrotron losses over time. For example, the power emitted by electrons is proportional to γ^2, so that higher-energy electrons radiatively cool much faster. Moreover, as the critical frequency is also proportional to γ^2, the spectra will become steeper at higher frequencies with time since the acceleration event. This *spectral aeging* can be used as a tool to infer the age of the jet, for example, by measuring the spectral differences between younger and older parts of the diffuse radio lobes enclosing jets(e.g., Harwood et al., 2015).

The radiating plasma can also become optically thick and absorb the synchrotron radiation it produces at lower frequencies. This process is known as *synchrotron self-absorption* (SSA). The spectrum of the self-absorbed radiation is determined by the location of the break frequency, ν_{SSA}. For a collection of electrons with a power law energy distribution with an index s, and assuming that the energies of absorbing electrons are much larger than the energies of interacting photons, the absorbed spectrum follows $F_\nu \propto \nu^{-5/2}$ for $\nu_{SSA} > \nu_{crit}$. However, if $\nu_{SSA} < \nu_{crit}$, the spectrum follows $F_\nu \propto \nu^2$ below ν_{SSA} and goes as ν^2 between ν_{SSA} and ν_{crit}. In any case, the spectrum always follows $\nu^{-(s-1)/2}$ for frequencies above the critical frequency.

It is important to note that the observed synchrotron power depends on both the electron Lorentz factor and the magnetic field (Eq. 1.2), which precludes estimating them individually from observations. Moreover, the uncertainty in the particle composition of the jet presents another problem in determining these parameters. If the ion/electron energy density ratio is η, then the total energy density of the particles would be $(1+\eta)U_e$, where U_e is the energy density of the electrons. At the minimum total energy of the system, the ratio of energy densities of the particles to that of the magnetic field can be shown to be (Longair, 2011):

$$\frac{(1+\eta)U_e}{U_B} = \frac{4}{3} \tag{1.4}$$

which is approximately equal to 1. This is condition is called as (near) *equipartition*. It is widely adopted to model emission from jets as it allows estimating the magnetic field and particle energies independently. However, it remains unclear what type often micro-physical processes drive the plasma to equipartition.

1.3.2 Inverse Compton Radiation

Apart from synchrotron radiation, the emission from the same electrons scattering ambient photons can significantly contribute contributor to the observed emission from jets. When a photon transfers its energy to a non-relativistic electron, it is called Compton scattering. However, if the electron moves at relativistic speeds, it can convert a portion of its kinetic energy to upscatter a photon from a lower frequency into a higher frequency. This process is called *inverse Compton (IC)* scattering. The inverse Compton radiation bears the same polarization as the radiation field that is being up scattered (Uchiyama et al., 2007). The total IC power radiated by a single electron by up scattering a radiation field of energy density U_{rad} is given by

$$P_{IC} = \frac{4}{3}\sigma_T \beta^2 \gamma^2 c U_{rad} \tag{1.5}$$

The ratio of the synchrotron to IC power would then become $P_{synch}/P_{IC} = U_B/U_{rad}$. The means, although both the synchrotron and IC processes are inevitable in a jet, it is the relative energy density of the magnetic field to the radiation field that determines the dominant emission mechanism. For a powerlaw distribution of electron energies with an index s, the IC spectrum also follows a powerlaw with an index of $(s-1)/2$, which is the same as the index for synchrotron emission. Furthermore, the synchrotron and IC powers both are $\propto \gamma^2$, making them indistinguishable purely using the observed spectra.

When the synchrotron electrons themselves IC scatter the radiation they produce, it leads to *synchrotron self Compton (SSC)* radiation. The SSC emission can also contribute back to the radiation field, leading to multiple SSC scatterings. SSC is regularly invoked to model the emission from the terminal regions of jets where it rams into the intergalactic medium (section **??**). Although it can amplify the emission, once the brightness temperature exceeds $T_b \sim 10^{12}$ K (e.g., Kellermann and Pauliny-Toth, 1969, see also Singal (2009) in this context) in the source's rest frame, synchrotron self-absorption dominates and sharply cools off the electrons.

1.3.3 Relativistic effects

It is now widely known that the parsec scale jets from AGN are highly relativistic, or their speeds are close to the speed of light. While the actual Lorentz factor of kpc scale jets remains uncertain, radio observations imply that the radio-emitting plasma is only mildly relativistic (e.g., Mullin and Hardcastle, 2009; Wardle and Aaron, 1997). Here I distinguish between the "jet-fluid", which is unclear, and the emitting plasma. For example, cold protons may be carrying the bulk kinetic energy of the jet, and we may observe radiation produced by accelerated electron plasma (e.g., at internal shocks), which may be slower than jet material carrying them. In general, observations of jets measure the *pattern-speed* of the emitting plasma, which may not always represent the actual jet speed. Hence for brevity, unless otherwise stated, I refer to emitting plasma's speed simply as the jet speed in the remainder of my thesis.

The radiation theory introduced in the previous sections is only applicable to sources moving at non-relativistic speeds and. At larger speeds, Doppler beaming effects become important. For an isotropically emitting source, which is generally the case for synchrotron emitters, moving with a bulk Lorentz factor $\Gamma = 1/\sqrt{1-\beta^2}$, the Doppler beaming factor, δ, is given by:

$$\delta = \frac{1}{\Gamma(1-\beta\cos\theta)} \tag{1.6}$$

where θ is the angle between the jet's velocity vector and our line of sight. A photon of frequency ν^{em} emitted in the rest frame of the source is related to the received frequency ν^{rec} by $\nu^{rec} = \delta E^{em}$. In other words, the photon's frequency will be *redshifted* for $\delta < 1$ while it is *blueshifted* for $\delta > 1$. If the source exhibits a powerlaw spectrum, ($F_\nu \propto \nu^{-\alpha}$), the received flux would be related to the flux in the emitting frame, F_ν^{em}, both evaluated at the observed frequency is given by (e.g., Dermer, 1995)

$$F_\nu^{rec} = F_\nu^{em}\delta^{p+\alpha} \tag{1.7}$$

where p=3 for a spherical source and p=2 for a cylindrical source[1]. This Doppler boosting of the emitted radiation is the main reason for one-sided appearance of closely-aligned jets (e.g., M87, shown in Fig. 1.1). For example, the observed flux from a source, with $\Gamma = 3$, $\alpha = 0.75$ and $\theta = 15°$, will be beaming by a factor of $\sim$140 when it approaches us while it is "de-beamed" by a factor of $\sim 10^{-3}$ when it recedes away from us. The beaming effect works differently in the case of IC radiation because the external photon field becomes anistropic in the rest frame

[1] This also applies to the case of a continuous flow, which can be considered as a long cylinder

of the plasma. The observed flux in this case is given by (e.g., Dermer, 1995; Georganopoulos et al., 2001).

$$F_\nu^{rec} = F_\nu^{em} \delta^{p+1+2\alpha} \tag{1.8}$$

where p assumes the same values as indicated for the synchrotron case.

The first confirmation of the relativistic nature of jets came from the observations of superluminal motions of jets on parsec scales of jetted-AGN using VLBI techniques (Whitney et al., 1971). This is a direct geometrical consequence of relativistic motion. When a radiating source mis highly relativistic, it can nearly catch up with its own radiation, and if it moves close to our line of sight, it can appear to move faster than the speed of light. Formally, the apparent transverse speed is given by

$$\beta_{app} = \frac{\beta \sin\theta}{1 - \beta\cos\theta} \tag{1.9}$$

The apparent speed attains its maximum when the motion is observed at a *critical angle*, $\cos\theta_c = \beta$. The critical angle also yields a lower limit on Γ, which is given by

$$\Gamma \geq \sqrt{\beta_{app}^2 + 1} \tag{1.10}$$

Conversely, by allowing $\beta \to 1$, which is the maximum allowed intrinsic speed, we can obtain the maximum viewing angle:

$$\cos\theta_{max} = \frac{\beta_{app}^2 - 1}{\beta_{app}^2 + 1} \tag{1.11}$$

For example, if a jet exhibits an apparent transverse motion of $\beta_{app} = 20$, it implies $\Gamma \geq 20.02$ with a maximum viewing angle $\theta \leq 5.7°$. Finally, thanks to the radio

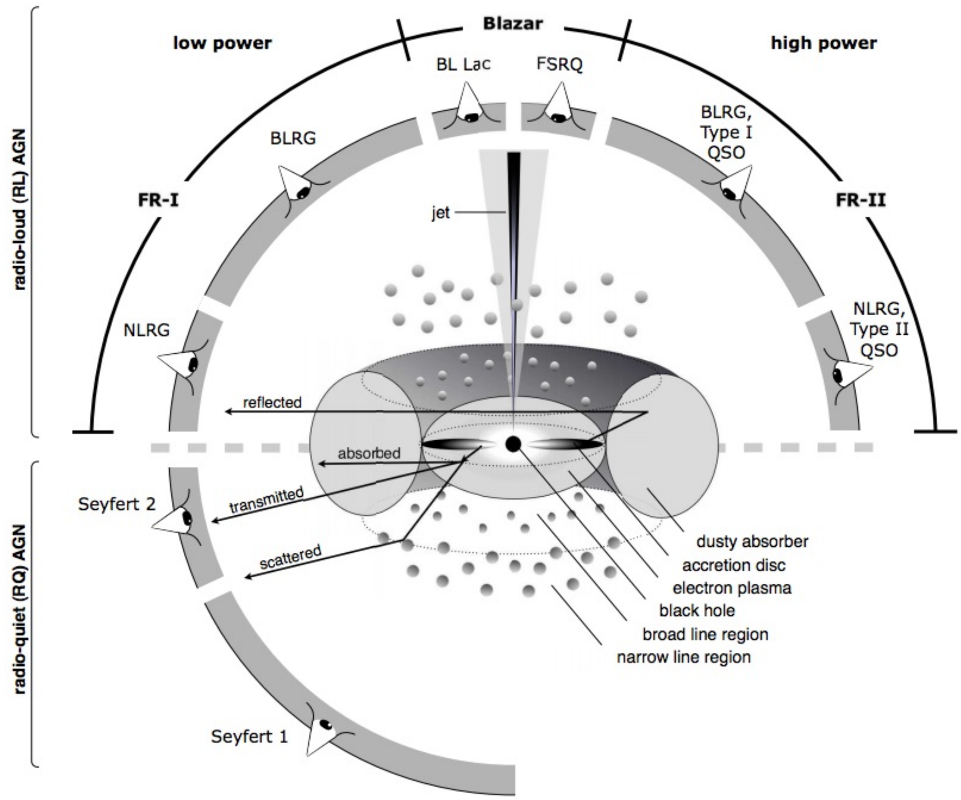

Figure 1.2: A simplified schema of the current model of the AGN, not drawn to scale. The taxonomy of the AGN is a result of the presence or absence of various components and observational effects. Figure reproduced from Beckmann and Shrader (2012).

telescopes such as the Very Long Baseline Array (VLBA), hundreds of superluminal sources are identified so far (e.g., Lister et al., 2018); they have significantly advanced our knowledge about jet physics.

1.4 Active Galactic Nuclei: The current model

Figure 1.2 shows a simplified view of the default AGN model. A SMBH at the center forms the *central engine*, accreting matter via an accretion disk. For powerful systems, the spectrum of the disk peaks in the optical/UV and is traditionally called the "big blue bump." The accretion disk photoionizes the neighboring high density and dust-free gas clouds, which leads to the production of strong emission lines. These clouds mostly occur within a parsec of the SMBH (Peterson, 2006); they move with roughly keplerian speeds, and, as a result, broaden the emission lines. Hence, this region is known as the broad-line region (BLR). The low-density, low velocity, ionized gas, residing a few hundred to thousands of parsecs away from the black hole, moves with slower speeds, and produces narrower emission lines. This region constitutes the narrow-line region (NLR). A dusty torus structure may also surround the black hole-disk system. When viewed edge-on, this torus obscures the emission from the BLR. Such sources lack broad emission lines and fall under the Type II class of AGN. If the AGN are observed face-on, the broad emission lines become visible, and are categorized as Type I AGN. This viewing angle based classification plays an important role in understanding the AGN, although it is clear that the torus is likely more complex and "clumpy" that what is shown here (see Hönig, 2019, and references there in).

1.4.1 AGN Taxonomy

AGN were classified, traditionally, as radio-loud and radio-quiet, in an empirical sense. The dividing factor was the ratio of radio to optical flux density (R). Those with $R \leq 10$ were classified radio-quiet (but are not radio-silent) and those above the limit radio-loud. However, this classification has been criticized in the recent times for its oversimplification (e.g., Padovani, 2016). For example, the emission in the optical band may be dominated by the jet itself, and can lead to $R < 10$, thereby incorrectly classifying sources as radio-quiet. Hence this distinction is not just taxonomic but an intrinsic one. It stems from the presence or absence of a jet (Padovani, 2017). Hence, in what follows, they would instead be referred to as jetted and non-jetted AGN, respectively.

1.4.1.1 Jetted AGN

Radio Galaxies (RG) are the initial detections of jetted AGN with identified optical counterparts (e.g., Baade and Minkowski, 1954). They are AGN with jets that are aligned away from our line of sight. RGs are further classified in to two types based on their optical spectra: broad line (BLRG), which display both broad and narrow emission lines, and narrow line (NLRG), which only display narrow lines (see Fig 1.2). Fanaroff and Riley (1974) found that the morphology of the large-scale jet occured in two main flavours and correlated with its low-frequency radio luminosity. It was later found that the same also exists in the radio-optical luminosity plane (Owen and Ledlow, 1994). The lower power Fanaroff-Riley Class I (FR I) jets display a plumy structure which fade away with distance from the *core*, which forms the base of the jet. The left panel in Fig. 1.3 shows a radio image of M84, a typical case of FR I jet. In contrast, the more powerful FR-II type jets, which are the main focus of my thesis, remain highly collimated and travel to much longer distances before they ram in to the inter-galactic medium terminating in a bright *hotspot* where the

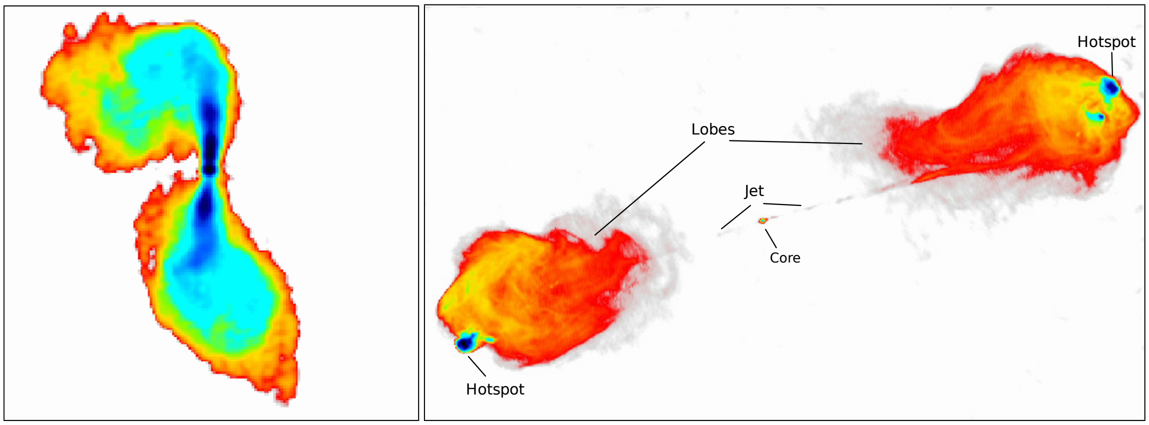

(a) M84, an FR I jet

(b) Cygnus A, an FR II jet

Figure 1.3: Typical example images for the FR I and II classes. (a) shows a VLA radio image of an FR-I source, M84, where the where the jet's brightness gradually decreases with increasing distance from the core (image taken from DRAGN website, http://www.jb.man.ac.uk/atlas/). (b) shows a a radio image of an FR-II source, Cygnus A. Two jets originate from the core and terminate in bright hotspots, feeding accelerated plasma into the radio lobes (image taken from NED, http://ned.ipac.caltech.edu).

electrons are re-accelerated before escaping into the lobes. It were these gaint radio-emitting lobes that appeared as extended structures in the initial sky surveys. In general, sources with luminosity at 1.4 GHz $L_{1.4GHz} < 5 \times 10^{25}$ W Hz^{-1} belong to the FR I class while most of those above the limit to the FR II class. Note that, Fanaroff and Riley (1974)originally divided sources into FR-I and FR-II classes using the luminosity at 178 MHz which is expected to be dominated by isotropic emission from the c

Quasars comprise the most powerful class of jetted-AGN with their jets aligned at relatively smaller angles than FR I/II sources. They are typically characterized by the presence of broad emission lines in the optical spectrum and high luminosity radio emission. Quasars are classified into Steep Radio Spectrum Quasars (SRSQ) and Flat Spectrum Radio Quasars (FSRQ). SRSQs are dominated by emission from their radio lobes, which usually have steep spectra (α >0.5). FSRQs, often referred to as *Blazars*, are dominated by emission from the cores, which usally have flatter spectra (α <0.5). Their jets aligned very close to our line of sight, and typically appear point-like in radio maps with their jets barely visible due to extreme foreshortening. They are are further divided into two classes: FSRQ, which display broad emission lines, and BL Lacertae objects (BL Lacs), which have featureless spectra. Under the primary unification scheme (e.g., Urry and Padovani, 1995), FSRQs and BL Lacs are the closely aligned counterparts of FR II and FR-I RGs, respectively. Blazars have the highest apparent luminosity of all AGN families with Doppler beaming capable of enhancing the intrinsic luminosity by a factor of up to 10^9. Historically, quasars were also classified into lobe-dominated quasars (LDQ) and core-dominated quasars (CDQ). LDQs (and FR II RGs) are mainly detected in low-frequency radio surveys which are dominated by isotropic emission from lobes. On the other hand, CDQs are mainly detected in high-frequency radio surveys which are dominated by emission from the cores.

1.4.1.2 Non-jetted AGN

These are the most common class of AGNs in the local universe, and Seyfert galaxies (Seyfert, 1943) were the first ones to be identified in this class. Seyfert conducted his research using the telescopes at Mt. Wilson, which also hosted prominent researchers indlucing Edward Hubble who pioneered extragalatic studies and Albert Michelson who worked on interfgerometry.

Typically, the Seyferts are distingusihed from other normal galaxies by their highly ionized emission lines and luminous cores. Similar to jetted-AGNs, the Seyfert galaxies are divided into two classes based on their optical spectra (Khachikian and Weedman, 1974): Seyfert I type, which display narrow and broad emission lines, and Seyfert II type, which only display narrow emission lines (see Fig. 1.2). Apart from the optical classification, the Sefyferts are also classified based on their X-ray emission, which relies on the intrinsic absorption in the soft X-ray band ($E \ll 5$ keV). A hydrogen absorption column density of $N_H = 10^{22}$ cm^{-2} draws the line between the type I and type II Seyferts. The ones above the threshold are strongly absorbed and fall into the type I class, while the ones below have lower absorption and fall into the type II class. Radio-quiet quasars are another type of non-jetted AGN. Similar to the Seyferts, the radio-quiet quasars are further divided in to type I and type II, which display broad lines and only narrow lines, respectively.

There may also be sources with a low luminosity that go undetected in the all-sky surveys. For example, the bolometric luminosity of Sagittarius A*, which is the black hole at the center of our Milky Way galaxy, is less than $L_{bol} = 10^{37}$ erg sec^{-1}.

Such emission would not be detected if it were to lie in a distant galaxy. It is believed that these sources may have experienced some activity in the past and are presently undergoing a quiescent phase.

1.4.2 The Central Engine

The idea of a black hole at the center of AGN was a groundbreaking one as it explained puzzling features of the AGN such as short variability time scales and extremely high luminosity (Lynden-Bell, 1969; Salpeter, 1964; Zel'dovich and Novikov, 1964). It is now widely believed that accretion on to an SMBH power all forms of AGN.

1.4.2.1 Detecting SMBH in AGN

Although the idea of an SMBH at the center of an AGN was rapidly adopted by the community, it took a long time to infer the presence of black holes. So indirect methods that revealed the gravitational influence of black holes on their surroundings became the key. For example, star trajectories around the presumed location of a black hole can be monitored to infer its presence. However, they typically orbit around SMBHs on sub-parsec scales. Hence, this method could only be applied to a few nearby galaxies that allowed telescopes like HST to track proper motions of individual stars. Indeed, the properties of the SMBH at our galaxy's center remain the most precise ever to be measured using this method (Ghez et al., 2008).

Reverberation mapping is another important technique that was developed in the 1990s (see Peterson and Horne (2004) for a review) to measure the properties of SMBHs. In the default picture of AGN, the continuum from the accretion disk ionizes the gas clouds in the BLR that, in turn, emit emission lines. Broader line-widths are expected from regions closer to the black hole because of faster speeds and stronger gravitational fields. Hence, any change in brightness of the continumm must also lead to a change in the brightness of the emission lines but with an associated time lag. Because any correlated events can only happen on timescales greater than the light-crossing time between two regions, these time lags place can be used to place an upper limit on the size of the BLR and also determine the mass of the black hole (Peterson and Horne, 2004).

Another key insight was gained in the 1990s, where it was found that the mass of a galaxy's SMBH correlates with the surrounding spheroidal distribution of stars known as the galactic bulge (Magorrian et al., 1998). The observed stellar velocity dispersion at the center of a galaxy is known to scale with its bulge mass. This dispersion is currently used to estimate the mass of the SMBHs and is known as the $M - \sigma$ relation (Ferrarese and Merritt, 2000; Gebhardt et al., 2000). Recently the Event Horizon Telescope provided a direct evidence of SMBH by imaging the central region of M87 (Event Horizon Telescope Collaboration et al., 2019).

1.4.2.2 Disk Accretion and the Eddington Limit

The accretion process is extremely efficient at converting the gravitational potential energy of infalling matter into radiation. "Spherical" type of accretion, commonly called *Bondi* accretion (Bondi, 1952), that was was the first type to be sturied. Bondi accretion is only a good approximation for isolated compact objects and is unlikely to be the main process behind AGN activity. It is because of the lack of angular momentum in spherical accretion: the particles do not have time to radiate their thermal energy before they fall in to the black hole. However, if the in-falling matter forms a disk while possessing angular momentum, its radiative efficiency can be significantly higher. In the case of objects like AGN, an accretion disk will be formed. The bolometric luminosity of the accretion disk is given by $L_{acc} = \eta \dot{M} c^2$, where $\dot{M}$ is the accretion rate and η is the radiative efficiency of the disk. The efficiency parameter η can range between 0.06 and 0.3 and is determined by several parameters including spin of the black hole, the type of accretion that are far from a clear understanding (Raimundo and Fabian, 2009).

In 1920s, Arthur Eddington noted that for a spherical mode of accretion, the radiation from the inner parts of the in-falling matter would exert pressure on the outer parts, thereby limiting the maximum achievable luminosity. The limiting luminosity depends on the type of the in-falling matter, which is generally taken to be ionized hydrogen in most astrophysical environments, and the mass of the black hole. It is called the *Eddington* luminosity. For a black hole that predominantly accretes ionized hydrogen, the Eddington luminosity (in ergs s^{-1}) is given by

$$L_{edd} \simeq 1.3 \times 10^{38} \frac{M}{M_\odot} \text{erg/s} \simeq 3 \times 10^4 \frac{M}{M_\odot} L_\odot \tag{1.12}$$

where $L_\odot$ is the solar luminosity. A bright quasar typically has a luminosity of $\sim 10^{13} L_\odot$, which then implies a black hole mass of $\geq 3 \times 10^8 M_\odot$, indicating the super massive nature of black holes powering AGN. Note that L_{edd} is derived assuming spherical accretion and may be inaccurate for real systems where matter orbiting around SMBHs is expected to for a disk. Multiple other processes can also influence the L_{edd}. For example, highly-ionized heavier elements in the infalling matter can decrease the luminosity by absorbing spectral lines. Conversely, low-ionized counterparts practically remain transparent to the outgoing radiation, increasing the luminosity. Furthermore, any anisotropy in the distribution of the in-falling matter will accordingly decrease L_{edd} (Frank et al., 2002). These limiting factors clearly indicate L_{edd} only provides an order of magnitude estimate for the limiting luminosity, and accreting rate may exceed this value as observed in multiple AGN (e.g., Liu et al., 2021; Wang et al., 2014) .

1.4.2.3 Jet launching

The precise means by which the jets are accelerated by SMBHs remain unclear as is the matter content of the jet plasma. Over the years, many published jet launching mechanisms have commonly assumed that the jets acquire their mass from a certain fraction of the accreting matter. However, they differ in whether or not the magnetic field is primarily responsible for ejecting the jet.

Pure hydrodynamic models based on winds from accretion disks such as those powered by binary black holes (e.g., Shakura and Sunyaev, 1973) have limited capabilities. They cannot accelerate the jets to relativistic speeds, generally seen in VLBI observations. In contrast, low-efficiency accretion flows may produce adequately relativistic outflows with reasonable collimation (Das, 1998; Rees et al., 1982). However, these models rely on some critical assumptions that are yet to be verified.

The current belief is that magnetic fields play an important role in launching the jet and collimating them. One observational aspect supporting this view is radio emission from jets, which, by definition, requires a magnetic field. Also, magnetic fields can naturally produce relativistic speeds and collimated outflows with large kinetic energies (e.g., Heinz and Begelman, 2000), making magnetic field models superior to pure hydrodynamic models.

The magnetic field models generally come in two flavors. They either harvest energy and angular momentum from the accretion disk (e.g., Blandford and Payne, 1982, BP), or from the spin of the black hole that threads the magnetic field at its horizon (e.g., Blandford and Znajek, 1977, BZ). For the BP mechanism, one would expect a tight correlation between the accretion power and jet power, which is observed in some Galactic systems (e.g., Willott et al., 1999). However, there is also evidence for correlation between black hole-spin and jet power (e.g., McClintock et al., 2013) with recent 3D relativistic magnetohydrodynamic simulations of jets supporting this scenario (Martí, 2019; McKinney, 2006; Tchekhovskoy et al., 2011).

Another important unknown is the particle composition of the jet. The material that transports energy and momentum from the parsec scales of the AGN out to kpc and Mpc scales is still uncertain. As mentioned, this material may not necessarily be the radiation-emitting plasma. For example, electrons with energies $\gamma \geq 2000$[2] would not survive until the tip of the jet (Harris and Krawczynski, 2007) and hence cannot be the energy carriers of a jet. A few possibilities for the jet material include cold (thermal) or hot (relativistic) protons, cold electrons/positrons, or Poynting flux (energy stored in magnetic fields). Although neutrons were also suggested as a candidate jet material (Dermer and Atoyan, 2004) it faced difficulties with jet formation and jet bending on kpc scales. Sikora and Madejski (2000) argued that protons are the main energy carriers of the jet but electrons (and positrons) outnumber them. (Sikora et al., 2005) extended this argument by suggesting that the Poynting flux dominates the jet initially and the particles would dominate later with protons mainly carrying the energy of the jet. Hoever, observations of FR II radio-lobes indicated that those jets are more likely to be dominated by pair plasma.

The location where the jet reaches its peak Lorentz factor is also uncertain. It could happen extremely close to the black hole, or the jet could be progressively accelerated while propagating away from the black hole (see Meier, 2003). The latter mode is commonly adopted because if the jet is accelerated close to the black hole, it will experience significant energy loss by inverse-Compton scattering (see section 1.3.2) of the ambient photon field, a phenomenon that is commonly known as the "Compton drag" effect. More detailed observations, theoretical studies, and numerical simulations are necessary to resolve these questions.

[2] $gamma = \frac{1}{\sqrt{(1-(v/c)^2}}$is the Lorentz factor

1.5 X-ray jets

"A curious straight ray lies in a gap in the nebulosity in p.a. 20°, apparently connected with the nucleus by a thin line of matter. The ray is brightest at its inner end which is 11″ from the nucleus", Curtis (1918) noted, while describing the optical image of an elliptical galaxy, *NGC 4486*. This is considered as the first-ever detection of an astrophysical jet which we now recognize as the jet from M87. While radio and optical telescopes detected several jets by 1990s, it took a few more years for them to be properly resolved in the X-rays.

The construction of X-rays observatories based on gas proportional counters began in the 1950s, and were able to X-ray emission from AGN around early 1960s and late 1970s. However, they could not resolve jets due to low angular resolution. Later, the *Einstein* X-ray observatory was launched in 1978; it had a resolution of ≈5″ and was able to resolve nearby jets from the core in nearby sources M87 (Schreier et al., 1982). The launch of *ROSAT* soon followed in 1990, which had similar capabilities but with higher sensitivity. It was able to detect other nearby jets, including, the hotspots from Cygnus A and 3C 390.3 (Almudena Prieto, 1997; Reynolds and Fabian, 1996). Nevertheless, the poor angular resolution of both observatories precluded the detection of jets from distant sources as they required sub-arcsecond resolution.

1.5.1 The Chandra X-ray Observatory

The dection of distant X-ray jets was made possible by *Chandra*, an X-ray observatory with an unprecendented angular resolution of $\sim$0.5$''$. *Chandra* observes the sky between the energy range of 0.2-10 keV and remains one of the biggest drivers for jet physics studies in the recent times. After *Chandra* was injected into the orbit, the ground team selected a distant quasar, PKS 0637-752, with a 100 kpc long radio jet, to calibrate the telescope. Because PKS 0637-752 was expected to be a bright point source in the X-rays, it was also going to serve as a calibrator for the telescope's in-focus measurements. However, with only a 2 ks exposure on this source, a faint bridge-like structure appeared to the west of its core, along the same position angle as the radio jet. This detection marked *Chandra's* first serendipitous discovery of an X-ray jet (Chartas et al., 2000). The left panel of Figure 1.4 shows a 100ks *Chandra* image of this source, while the right panel shows its 8.6 GHz radio image.

The radio-to-X-ray spectrum of FR-I jets is generally consistent with a single synchrotron component (e.g., Hardcastle et al., 2003; Marshall et al., 2002) suggesting that a single electron population with a powerlaw distribution of energies produce the emission via synchrotron mechanism (for a notable exeception, see Meyer et al., 2018). However, nearly in all the sources with an FR II-type jet like PKS 0637-752, the observed X-ray emission is a few orders of magnitude brighter than an extension to the radio and optical (if present) spectrum (e.g., Hogan et al., 2011; Marshall et al., 2005; Marshall et al., 2011; Marshall et al., 2018; Sambruna et al., 2004),

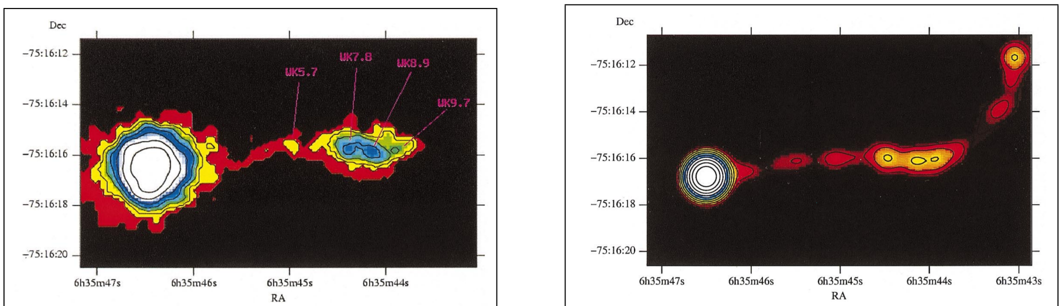

(a) *Chandra* X-ray image

(b) ATCA 8.6GHz radio image

Figure 1.4: The X-ray and radio images of PKS0637-752, the first detection of an X-ray jet by *Chandra*. Image taken from Chartas et al. (2000)

clearly requiring a second spectral component. Following (Breiding et al., 2017), I refer to these jets as "Multi Spectral component (MSC)" jets. The left panel of Figure 1.5 shows the observed spectrum of a discrete feature or a "knot", W7.8, in PKS 0637-752 as an example. The solid line indicates the low energy synchrotron spectrum with no detectable level of X-ray flux. Moreover, invoking thermal processes for the genesis of X-rays in this jet implied unrealistic electron densities and higher than observed rotation measures (Schwartz et al., 2000). While SSC flux under equipartition fell short of the observed X-ray flux at least by a factor of 100, IC scattering the cosmic microwave background CMB (IC/CMB) by a non-relativistic jet underpredicted it by about three orders of magnitude (Chartas et al., 2000).

1.5.2 The IC/CMB model

A few months after *Chandra* detected its first jet, two independent groups reproduced the X-rays in PKS 0637-752 with IC/CMB by requiring its jet to be

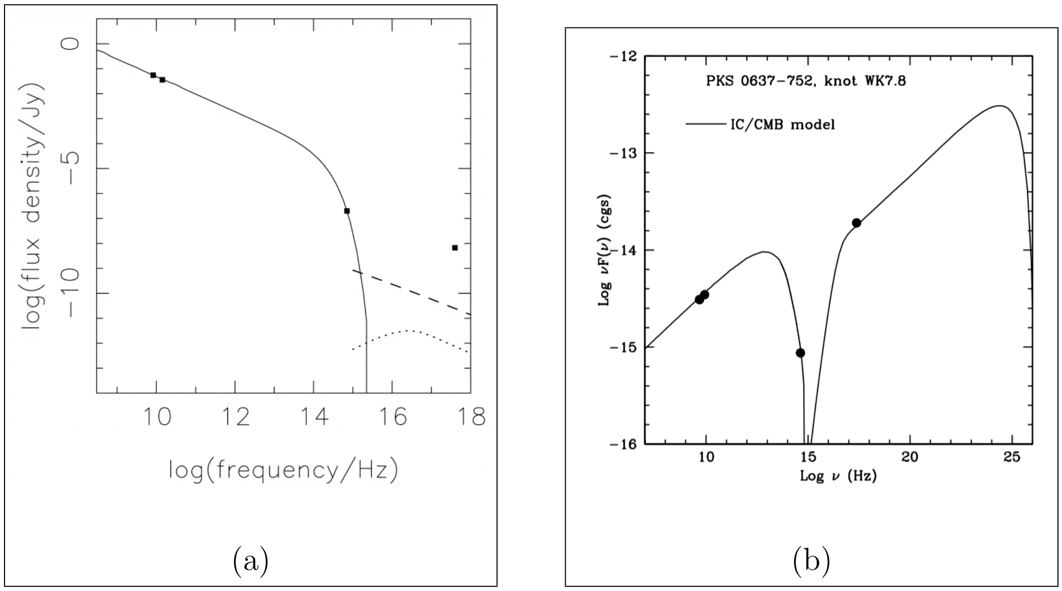

Figure 1.5: (a) The spectrum of knot W7.8 of PKS0637-752 where the solid line is the synchrotron component. Under equipartition condition, the dashed line indicates the SSC component while the dotted line, the inverse-Compton component from a non-relativistic jet, and both the mechanisms fail to account for the observed X-ray emission. Image taken from Chartas et al. (2000) (b) The Spectral energy distribution (SED) of knot W7.8 of PKS 0637-752. The X-ray emission can be explained by IC/CMB if the jet is closely aligned and highly relativistic, and the up-scattering electrons have low energies (much lower than what is traced by the radio-optical spectrum). Image taken from Tavecchio et al. (2000).

highly relativistic and closely aligned to our line of sight (Celotti et al., 2001; Tavecchio et al., 2000). The right panel of Fig. 1.5 shows the SED of the W7.8 knot in PKS 0637-752 with an IC/CMB component consistent with the obsereved X-ray flux. Until recently, the IC/CMB model remained the leading explanation for X-ray emission from MSC jets (e.g., Kharb et al., 2012; Miller et al., 2006; Sambruna et al., 2004, 2006). However, it failed to describe multiple spectral and structural characteristics of MSC jets.

1.5.3 Issues with the IC/CMB model

Under equipartition conditions, electrons tracing the GHz spectrum typically have $\gamma \sim 10^4$, much larger than the energies required by IC/CMB ($\gamma \sim 30-100$) to produce X-rays. Extending the electron energy distribution (EED) to low energies requires introducing a significantly larger number of electrons into the jet and may make its kinetic power to exceed the Eddington luminosity (Dermer and Atoyan, 2004). Moreover, the EEDs need an *ad-hoc* cutoff at low energies (e.g., $\gamma_{min} = 10$) to prevent overproducing the optical emission. Even if the IC/CMB electrons exist in jets, their synchrotron emission possibly lies below the ionospheric cutoff making it impossible to detect them with the modern day telescopes. In contrast, low-frequency radio maps of the lobes of radio galaxies, which are non-relativistic and emit isotropically with $\gamma \sim 10^3$, provide direct evidence for IC/CMB mode of X-ray emission (e.g., Feigelson et al., 1995).

Beside low-energy electons, the radio-optical emitting electrons will also up-scatter the CMB photons to produce GeV emission. Its flux-level is predetermined by the requirement of reproducing the X-ray emission (Georganopoulos et al., 2006). Properly, the SED of the IC component is a scaled and translated version of its low-energy counterpart. However, upper limits on GeV emission from the jets in many quasars, including PKS 0637-752, obtained by the *Fermi* imply much lower values than the predicted level (Breiding et al., 2017; Meyer et al., 2015).

Since the radio and X-rays are produced by the same electrons, their spectral indices are expected to match. While low-count statistics of the X-ray spectra prevent an accurate comparison between X-ray and radio spectral indices for many jets, high-sensitivity *Chandra* observations of a well studied nearby jet, 3C 273, indicate a clear disagreement between X-ray/radio spectral indices (Jester et al., 2006).

Another argument against IC/CMB comes from UV polarimetry of PKS 1136-135, a unique source where, unlike in most of the MSC jets, the UV emission lies on the low-energy tail of the second spectal component. For IC/CMB to produce the observed UV to X-ray spectrum, the upscattering electrons must have $\gamma \sim$ few for the UV and $\gamma \sim 100$ for the X-rays (Uchiyama et al., 2007). Because the CMB is unpolarized, X-rays are expected to be unpolarized UV emission to be slightly (few percent) polarized (McNamara et al., 2009; Uchiyama, 2008). However, the fractional polarization in the UV exceeds ∼30% in several knots, ruling out IC/CMB (Cara et al., 2013).

The knotty morphology observed in several X-ray jets presents a problem for the IC/CMB model (e.g., Clautice et al., 2016; Jester et al., 2006; Sambruna et al., 2004; Siemiginowska et al., 2007). While the mechanism producing knots is unknown, the large radiative cooling times of the X-ray emitting electrons ($\geq 10^6$ years, e.g., Harris and Krawczynski, 2006) implies no significant X-ray brightness variations must be observed along the jet as opposed to the observed knots with differing brightnesses. Although separate moving blobs of plasma with large bulk Lorentz factors ($\Gamma > 10$) can still produce X-rays knots emitting via IC/CMB (Tavecchio et al., 2003), optical proper motions in the knots of nearby jets indicate much smaller values ($\Gamma < 2.9$ in 3C 273, e.g., Meyer et al., 2016). Moreover, assuming moving knots are made of several smaller clumps can explain X-ray flux variations in knots via adiabatic losses. However, these losses may produce a large poulation of electrons capable of overproducing the optical emission via IC/CMB (Stawarz et al., 2004).

Long cooling times also imply multiple other properties. First, no variability in the X-ray flux would be expected on human time scales unlike a knot in Pictor A that varied significantly in a few years (Marshall et al., 2010). Second, because of the relatively smaller lifetimes of GHz radio-emitting electrons, as noted by Worrall (2009), we should expect the X-rays to extend beyond the radio or at least be co-spatial, appearing as if being emitted from a "single zone" in the jet. However, the X-rays peak and decay before the radio in many knots of MSC jets (e.g., Clautice et al., 2016; Kataoka et al., 2008; Siemiginowska et al., 2007; Worrall, 2009; Worrall and Birkinshaw, 2005), generally manifesting as peak-to-peak positional *offsets* between X-rays and radio. Figure 1.6 shows the X-ray image of 3C 111, overlaid with 8.4 GHz radio contours. Offsets can be seen, for example, in knots K9, K30, K45. Although we are far from understanding how offsets are produced, they place an important constraint on the emission morphology and, in turn, the X-ray emission mechanism: the bulk of the X-ray and radio emissions are produced in different zones of the jet, contrary to IC/CMB's single zone operation. It is important to note that this

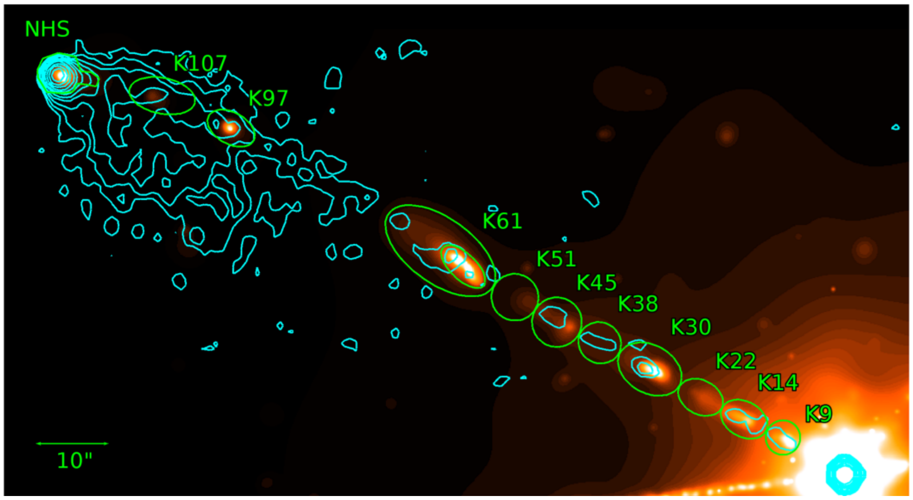

Figure 1.6: A smoothed X-ray image of 3C111, overlaid with the VLA 8.4 GHz radio contours. The X-rays peak and decay before the radio in multiple knots including K9, K30, K45, K61, which appear as peak to peak offsets. Image taken from Clautice et al. (2016)

constraint applies independent of the emission mechanism.

1.5.4 Modified IC/CMB and Alternatives

A major issue with the IC/CMB model from the beginning was its requirement for the jet to remain relativictic ($\Gamma \sim 10$) even on kpc scales. In contrast, all radio-based studies on large scale jets implied that radio jets only mildly relativistic ($\Gamma \lesssim 1.5$, e.g., Mullin and Hardcastle, 2009; Wardle and Aaron, 1997). One clue came from the observations of X-ray fluxes that decreased with distance from the core. Hardcastle (2006) noted that although IC/CMB coupled with jet deceleration can explain this decline, the cold matter required to entrain the jet in many cases is implausibly high. The author suggested that a transverse velocity structure (e.g., a fast X-ray spine enclosed by a slow radio sheath) must exist in MSC jets for IC/CMB to be still viable. Stratified velocity structures are not new and are established in many FR I jets (e.g., Canvin and Laing, 2004; Laing and Bridle, 2004). While a spine-sheath structure is detected in the parsec scale jets of MSC jets (e.g., Bruni et al., 2021), its presence is yet to be confirmed on kpc scales.

One of the first invocations of spine-sheath models for MSC jets was made in the case of 3C 273. Although it satisfactority reproduced the observed X-ray fluxes from knots, it required unrealistic bulk Lorentz factors ($\Gamma \sim$50-100) for the spine. Moreover, as mentioned, it could not explain the disagreement between X-ray radio spectral indices. Siemiginowska et al. (2007) considered a variant for the case of PKS 1127-145 with a "proper" jet consisting of a regular spine and sheath, and a "sheath" representing an extension to the jet's boundary layer. Although this model explained multiple aspects of the broadband emission from the knots in PKS 1127-145, it sometimes required extreme changes in the magnetic fields between knots. Nevertheless, the evaluated two-zone IC/CMB models lack a natural explanation for the observed offsets.

Motivated by the problems with IC/CMB model, several workers in the field sided with an alternative, the synchrotron mechansim (e.g., Clautice et al., 2016; Hardcastle, 2006; Jester et al., 2006). Producing X-ray via synchrotron would require a high-energy electron population with energies that extend up to 100 TeV (much lager than $\sim$ 1 TeV electrons that produce radio/optical emission). While this explanation relaxes many constraints imposed by the IC/CMB model, for example, close alignments or large bulk Lorentz factors, it also requires cutoff at a few TeV to avoid overproducing optical emission. Moreover, as noted by (Schwartz et al., 2000), introducing a second synchrotron population is ad-hoc in nature (Schwartz et al., 2000)–we have no explanation for its existence. Dermer and Atoyan (2002) suggested that a single electron population producing radio-to-X-ray emission via synchrotron emission can devlop a harder tail at X-ray wavelengths owing to inefficient IC losses in the Klein-Nishina regime, resulting in a two component SED. This model requires the radiative losses be more pronounced in IC compared to synchrotron. Hadronic models may also produce X-rays via synchtrotron, eliminating the need to introduce a second population of electrons (e.g., Aharonian, 2002; Petropoulou et al., 2017). However, these models require a large proportion of protons, which in turn implies large jet powers, and magnetic fields on the orders of several Gauss, which are difficult to produce hundreds of kpcs away from the central engine.

The cooling times of X-ray emitting synchrotron electrons are on the order of a few years (Harris and Krawczynski, 2006). That means, presence of X-ray knots on hundreds of kpc away from the central engine requires *in-situ* acceleration of the electrons. Internal shocks (e.g., Kataoka et al., 2008; Stawarz et al., 2004) or acceleration in a shear turbulent layer (e.g., Ostrowski et al., 2002), for instance, can re-accelerate electrons, but the exact mechanism is not quite clear.

1.5.5 Knot and Offset Formation

Besides the uncertain X-ray emission mechanism, the lack of knowledge on how knots form introduces additonal uncertainty in modeling X-rays from MSC jets. For example, as mentioned, it is unclear whether X-ray and radio knots share the same bulk Lorentz factors. Furthermore, the applicability of equipartition conditions to knots is uncertain. It is reasonable to assume that radio lobes, which remain unperturbed for most of its extent, converge towards equipartition. However, knots, which can represent sites of freshly accelerated/accelerating plasma or parts of the jet perturbed by unknown means, may experience enhanced particle or magnetic field densities and may be far from eqipartition.

One possibility is that knots represent stationary re-confinement shocks driven by external pressure gradients(e.g., Komissarov and Falle, 1998), which, although, lacks a way to explain offsets. Alternatively, knots could be separate faster moving blobs of the plasma, produced by modulated activity in the central engine (e.g., Bridle et al., 1986, 1989; Clarke et al., 1992; Stawarz et al., 2004). A forward-reverse shock may then develop at the downstream tip of the blob, producing X-ray (synchrotron or IC/CMB) and radio emission (Stawarz et al., 2004). The observed similarities in the knot sizes across multiple radio frequencies and roughly periodically spaced knots in several jets support this model. (Kataoka et al., 2008) noted in a detailed study of a nearby jet, 3C 353, it is unclear why/how the two shocks produce seemingly different electron populations. They suggested the knots are instead heavy and slow moving blobs of plasma (still produced by modulated jet activity), embedded in a faster and lighter outerflow. A reverse shock can develop at the upstream end of the blob where it interacts with the outerflow, producing X-rays, while the blob coincides with the radio knot. However, this implies a volume-like emission geometry for radio contrary to surface-like indicated by several radio observations

(e.g., Swain et al., 1998)

While the IC/CMB models lack any offset producing mechanism, the synchrotron models can, in princple, accommodate offsets at the price of manually moving the X-ray emission zone away from its radio counterpart. In addition to the slow moving knot model introduced by Kataoka et al. (2008), offsets can be produced at bends in the jet where an intial strong shock produces X-rays, while a much weaker shock downstream of the jet produces radio (Worrall and Birkinshaw, 2005). Alternatively, offsets may result when accelerated plasma, initially emitting X-rays, emits gradually at longer wavelengths due to synchrotron loses while advecting downstream. This model implies offsets of about 100 kpc, much larger than the observed offsets of a few kpc (e.g., Clautice et al., 2016; Siemiginowska et al., 2007). Although they can be reduced by introducing additonal adiabatic losses due to a laterally expanding jet, the required expansion rates are much larger than what is observed (e.g., Kataoka et al., 2008; Swain et al., 1998).

The multi-TeV electrons in the synchrotron model will inevitably upcatter CMB photons to produce TeV radiation. These TeV photons can heat the intergalactic medium via plasma instabilities (e.g., Broderick et al., 2012; Chang et al., 2012) that can suppress the late-formation of dwarf galaxies (Pfrommer et al., 2012). They can also produce the intergalactic magnetic field and the extra galactic gamma ray background (Blandford et al., 2019; Broderick et al., 2012). Hence, if the synchrotron model is applicable to MSC jets, it may be an important clue to understand the structure formation in the universe. While the IC/CMB model is not ruled out completely for all jets, it is unclear whether a pure synchrotron can be preferrerd over it. Moreover, uncertainty in the knot formation mechanism makes the situation even more unclear. Nonetheless, if the single-zone IC/CMB model is correct, it would imply significantly larger jet powers and enormous differences in the environmental impact of jets compared to synchrotron-flavored jets.

1.6 This Thesis

Our understanding of the cosmos emerged from simple speculations about gas clouds in the sky to complex processes around black holes driving relativistic jets to millions of parsecs. Although the last few decades have witnessed substantial theoretical and numerical advances in jet physics, several questions such as how SMBHs accrete matter and launch jets, how they remain collimated, how the AGN activity is modulated, what the jets are composed of, how large scale jets produce X-rays, still remain open.

In the work presented here, in addition to spectral information, I characterize and use offsets of knots in a large sample of MSC jets to constrain their X-ray emission and knot formation mechanisms. In Chapter 2, largely drawn from Reddy et al. (2021), I describe a novel application of a statistical tool to detect offsets in low-count X-ray observations, where Poisson fluctuations and emission from nearby point sources previously precluded such an analysis. In Chapter 3, I extend this approach to a much larger sample of high-count X-ray jets to study trends in offsets and spectral data. This chapter is drawn from a forthcoming publication Reddy et al. (2022) and forms the heart of my theis. In Chapter 4, I will summarize the results of my thesis and describe possible future directions.

Bibliography

F. Aharonian. Proton-synchrotron radiation of large-scale jets in active galactic nuclei. *Monthly Notices of the Royal Astronomical Society*, 332(1):215–230, 2002.

M. Almudena Prieto. Extended x-ray emission associated with the northern hotspot of. *Monthly Notices of the Royal Astronomical Society*, 284(3):627–632, 1997.

R. J. Assef, D. Stern, G. Noirot, H. D. Jun, R. M. Cutri, and P. R. M. Eisenhardt. The WISE AGN catalog. *The Astrophysical Journal Supplement Series*, 234(2): 23, jan 2018. doi: 10.3847/1538-4365/aaa00a. URL https://doi.org/10.3847/1538-4365/aaa00a.

W. Baade. Polarization in the jet of messier 87. *The Astrophysical Journal*, 123: 550–551, 1956.

W. Baade and R. Minkowski. On the Identification of Radio Sources. ApJ, 119:215, Jan 1954. doi: 10.1086/145813.

T. W. Backhouse. nebula in Andromeda and Nova, 1885. MNRAS, 48:108, Jan. 1888. doi: 10.1093/mnras/48.3.108.

V. Beckmann and C. Shrader. Agn types and unification. *Active Galactic Nuclei (Wiley-VCH Verlag GmbH and Co. KGaA)*, 89, 2012.

A. S. Bennett and F. G. Simth. The Preparation of the Revised 3C Catalogue of Radio Sources. *Monthly Notices of the Royal Astronomical Society*, 125(1): 75–86, 07 1962. ISSN 0035-8711. doi: 10.1093/mnras/125.1.75. URL https://doi.org/10.1093/mnras/125.1.75.

R. Blandford and A. Königl. Relativistic jets as compact radio sources. *The Astrophysical Journal*, 232:34–48, 1979.

R. Blandford and D. Payne. Hydromagnetic flows from accretion discs and the production of radio jets. *Monthly Notices of the Royal Astronomical Society*, 199 (4):883–903, 1982.

R. Blandford, D. Meier, and A. Readhead. Relativistic jets from active galactic nuclei. *Annual Review of Astronomy and Astrophysics*, 57:467–509, 2019.

R. D. Blandford and R. L. Znajek. Electromagnetic extraction of energy from kerr black holes. *Monthly Notices of the Royal Astronomical Society*, 179(3):433–456, 1977.

H. Bondi. On spherically symmetrical accretion. *Monthly Notices of the Royal Astronomical Society*, 112(2):195–204, 1952.

P. Breiding, E. T. Meyer, M. Georganopoulos, M. Keenan, N. DeNigris, and J. Hewitt. Fermi non-detections of four x-ray jet sources and implications for the ic/cmb mechanism. *The Astrophysical Journal*, 849(2):95, 2017.

A. Bridle, R. Perley, and R. Henriksen. Collimation and polarization of the jets in 3c 219. *The Astronomical Journal*, 92:534–545, 1986.

A. H. Bridle and R. A. Perley. Extragalactic radio jets. *Annual review of astronomy and astrophysics*, 22(1):319–358, 1984.

A. H. Bridle, E. B. Fomalont, G. G. Byrd, and M. J. Valtonen. The unusual radio galaxy 3c 288. *The Astronomical Journal*, 97:674–685, 1989.

A. E. Broderick, P. Chang, and C. Pfrommer. The cosmological impact of luminous tev blazars. i. implications of plasma instabilities for the intergalactic magnetic field and extragalactic gamma-ray background. *The Astrophysical Journal*, 752 (1):22, 2012.

G. Bruni, J. L. Gómez, L. Vega-García, A. P. Lobanov, A. Fuentes, T. Savolainen, Y. Y. Kovalev, M. Perucho, J. M. Martí, J. M. Anderson, P. G. Edwards, L. I. Gurvits, M. M. Lisakov, A. B. Pushkarev, K. V. Sokolovsky, and J. A. Zensus. RadioAstron reveals a spine-sheath jet structure in 3C 273. A&A, 654:A27, Oct. 2021. doi: 10.1051/0004-6361/202039423.

J. Canvin and R. Laing. Relativistic models of two low-luminosity radio jets: B2 0326+ 39and b2 1553+ 24. *Monthly Notices of the Royal Astronomical Society*, 350(4):1342–1365, 2004.

M. Cara, E. S. Perlman, Y. Uchiyama, C. C. Cheung, P. S. Coppi, M. Georganopoulos, D. M. Worrall, M. Birkinshaw, W. B. Sparks, H. L. Marshall, et al. Polarimetry and the high-energy emission mechanisms in quasar jets: The case of pks 1136–135. *The Astrophysical Journal*, 773(2):186, 2013.

A. Celotti, G. Ghisellini, and M. Chiaberge. Large-scale jets in active galactic nuclei: multiwavelength mapping. *Monthly Notices of the Royal Astronomical Society*, 321(1):L1–L5, 2001.

P. Chang, A. E. Broderick, and C. Pfrommer. The cosmological impact of luminous tev blazars. ii. rewriting the thermal history of the intergalactic medium. *The Astrophysical Journal*, 752(1):23, 2012.

G. Chartas, D. M. Worrall, M. Birkinshaw, M. Cresitello-Dittmar, W. Cui, K. Ghosh, D. Harris, E. Hooper, D. Jauncey, D.-W. Kim, et al. The chandra x-ray observatory resolves the x-ray morphology and spectra of a jet in pks 0637–752. *The Astrophysical Journal*, 542(2):655, 2000.

H. Chiu. Gravitational collapse. *Publications of Goddard Space Flight Center*, page 13, 1964.

E. Churazov, S. Sazonov, R. Sunyaev, W. Forman, C. Jones, and H. Böhringer. Supermassive black holes in elliptical galaxies: switching from very bright to very dim. *Monthly Notices of the Royal Astronomical Society: Letters*, 363(1):L91–L95, 2005.

D. A. Clarke, A. H. Bridle, J. O. Burns, R. A. Perley, and M. L. Norman. Origin of the structures and polarization in the classical double 3c 219. *The Astrophysical Journal*, 385:173–187, 1992.

D. Clautice, E. S. Perlman, M. Georganopoulos, M. L. Lister, F. Tombesi, M. Cara, H. L. Marshall, B. Hogan, and D. Kazanas. The Spectacular Radio-near-ir-x-ray jet of 3c 111: the X-ray Emission Mechanism and jet Kinematics. *Astrophys. J.*, 826(2):109, 2016. doi: 10.3847/0004-637X/826/2/109.

M. Cohen, W. Cannon, G. Purcell, D. Shaffer, J. Broderick, K. Kellermann, and D. Jauncey. The small-scale structure of radio galaxies and quasi-stellar sources at 3.8 centimeters. *The Astrophysical Journal*, 170:207, 1971.

H. D. Curtis. Descriptions of 762 nebulae and clusters photographed with the crossley reflector. *Publications of Lick Observatory*, 13:9–42, 1918.

T. Das. Observational evidence for black holes in the universe. ed. sk chakrabarti, 1998.

C. D. Dermer. On the beaming statistics of gamma-ray sources. *The Astrophysical Journal*, 446:L63, 1995.

C. D. Dermer and A. Atoyan. Nonthermal radiation processes in x-ray jets. *The Astrophysical Journal Letters*, 611(1):L9, 2004.

C. D. Dermer and A. M. Atoyan. X-ray synchrotron spectral hardenings from compton and synchrotron losses in extended chandra jets. *The Astrophysical Journal Letters*, 568(2):L81, 2002.

D. O. Edge, J. R. Shakeshaft, W. B. McAdam, J. E. Baldwin, and S. Archer. A survey of radio sources at a frequency of 159 Mc/s. MmRAS, 68:37–60, Jan. 1959.

Event Horizon Telescope Collaboration, K. Akiyama, A. Alberdi, W. Alef, K. Asada, R. Azulay, A.-K. Baczko, D. Ball, M. Baloković, J. Barrett, D. Bintley, L. Blackburn, W. Boland, K. L. Bouman, G. C. Bower, M. Bremer, C. D. Brinkerink, R. Brissenden, S. Britzen, A. E. Broderick, D. Broguiere, T. Bronzwaer, D.-Y. Byun, J. E. Carlstrom, A. Chael, C.-k. Chan, S. Chatterjee, K. Chatterjee, M.-T. Chen, Y. Chen, I. Cho, P. Christian, J. E. Conway, J. M. Cordes, G. B. Crew, Y. Cui, J. Davelaar, M. De Laurentis, R. Deane, J. Dempsey, G. Desvignes, J. Dexter, S. S. Doeleman, R. P. Eatough, H. Falcke, V. L. Fish, E. Fomalont, R. Fraga-Encinas, W. T. Freeman, P. Friberg, C. M. Fromm, J. L. Gómez, P. Galison, C. F. Gammie, R. García, O. Gentaz, B. Georgiev, C. Goddi, R. Gold, M. Gu, M. Gurwell, K. Hada, M. H. Hecht, R. Hesper, L. C. Ho, P. Ho, M. Honma, C.-W. L. Huang, L. Huang, D. H. Hughes, S. Ikeda, M. Inoue, S. Issaoun, D. J. James, B. T. Jannuzi, M. Janssen, B. Jeter, W. Jiang, M. D. Johnson, S. Jorstad, T. Jung, M. Karami, R. Karuppusamy, T. Kawashima, G. K. Keating, M. Kettenis, J.-Y. Kim, J. Kim, J. Kim, M. Kino, J. Y. Koay, P. M. Koch, S. Koyama, M. Kramer, C. Kramer, T. P. Krichbaum, C.-Y. Kuo, T. R. Lauer, S.-S. Lee, Y.-R. Li, Z. Li, M. Lindqvist, K. Liu, E. Liuzzo, W.-P. Lo, A. P. Lobanov, L. Loinard, C. Lonsdale, R.-S. Lu, N. R. MacDonald, J. Mao, S. Markoff, D. P. Marrone, A. P. Marscher, I. Martí-Vidal, S. Matsushita, L. D. Matthews, L. Medeiros, K. M. Menten, Y. Mizuno, I. Mizuno, J. M. Moran, K. Moriyama, M. Moscibrodzka, C. Müller, H. Nagai, N. M. Nagar, M. Nakamura, R. Narayan, G. Narayanan, I. Natarajan, R. Neri, C. Ni, A. Noutsos, H. Okino, H. Olivares, G. N. Ortiz-León, T. Oyama, F. Özel, D. C. M. Palumbo, N. Patel, U.-L. Pen, D. W. Pesce, V. Piétu, R. Plambeck, A. PopStefanija, O. Porth, B. Prather, J. A. Preciado-López, D. Psaltis, H.-Y. Pu, V. Ramakrishnan, R. Rao, M. G. Rawlings, A. W. Raymond, L. Rezzolla, B. Ripperda, F. Roelofs, A. Rogers, E. Ros, M. Rose, A. Roshanineshat, H. Rottmann, A. L. Roy, C. Ruszczyk, B. R. Ryan, K. L. J. Rygl, S. Sánchez, D. Sánchez-Arguelles, M. Sasada, T. Savolainen, F. P. Schloerb, K.-F. Schuster, L. Shao, Z. Shen, D. Small, B. W. Sohn, J. SooHoo, F. Tazaki, P. Tiede, R. P. J. Tilanus, M. Titus, K. Toma, P. Torne, T. Trent, S. Trippe, S. Tsuda, I. van Bemmel, H. J. van Langevelde, D. R. van Rossum, J. Wagner, J. Wardle, J. Weintroub, N. Wex, R. Wharton, M. Wielgus, G. N. Wong, Q. Wu, K. Young, A. Young, Z. Younsi, F. Yuan, Y.-F. Yuan, J. A. Zensus, G. Zhao, S.-S. Zhao, Z. Zhu, J.-C. Algaba, A. Allardi, R. Amestica, J. Anczarski, U. Bach, F. K. Baganoff, C. Beaudoin, B. A. Benson, R. Berthold, J. M. Blanchard, R. Blundell, S. Bustamente, R. Cappallo, E. Castillo-Domínguez, C.-C. Chang, S.-H. Chang, S.-C. Chang, C.-C. Chen, R. Chilson, T. C. Chuter, R. Córdova Rosado, I. M. Coulson, T. M. Crawford, J. Crowley, J. David, M. Derome, M. Dexter, S. Dornbusch, K. A. Dudevoir, S. A. Dzib, A. Eckart, C. Eckert, N. R. Erickson, W. B. Everett, A. Faber, J. R. Farah, V. Fath, T. W. Folkers, D. C. Forbes, R. Freund, A. I. Gómez-Ruiz, D. M. Gale, F. Gao, G. Geertsema, D. A. Graham, C. H. Greer, R. Grosslein, F. Gueth, D. Haggard, N. W. Halverson, C.-C. Han, K.-C. Han, J. Hao, Y. Hasegawa, J. W. Henning, A. Hernández-Gómez, R. Herrero-Illana, S. Heyminck, A. Hirota, J. Hoge, Y.-D. Huang, C. M. V. Impellizzeri, H. Jiang, A. Kamble, R. Keisler, K. Kimura, Y. Kono, D. Kubo, J. Kuroda,

R. Lacasse, R. A. Laing, E. M. Leitch, C.-T. Li, L. C. C. Lin, C.-T. Liu, K.-Y. Liu, L.-M. Lu, R. G. Marson, P. L. Martin-Cocher, K. D. Massingill, C. Matulonis, M. P. McColl, S. R. McWhirter, H. Messias, Z. Meyer-Zhao, D. Michalik, A. Montaña, W. Montgomerie, M. Mora-Klein, D. Muders, A. Nadolski, S. Navarro, J. Neilsen, C. H. Nguyen, H. Nishioka, T. Norton, M. A. Nowak, G. Nystrom, H. Ogawa, P. Oshiro, T. Oyama, H. Parsons, S. N. Paine, J. Peñalver, N. M. Phillips, M. Poirier, N. Pradel, R. A. Primiani, P. A. Raffin, A. S. Rahlin, G. Reiland, C. Risacher, I. Ruiz, A. F. Sáez-Madaín, R. Sassella, P. Schellart, P. Shaw, K. M. Silva, H. Shiokawa, D. R. Smith, W. Snow, K. Souccar, D. Sousa, T. K. Sridharan, R. Srinivasan, W. Stahm, A. A. Stark, K. Story, S. T. Timmer, L. Vertatschitsch, C. Walther, T.-S. Wei, N. Whitehorn, A. R. Whitney, D. P. Woody, J. G. A. Wouterloot, M. Wright, P. Yamaguchi, C.-Y. Yu, M. Zeballos, S. Zhang, and L. Ziurys. First M87 Event Horizon Telescope Results. I. The Shadow of the Supermassive Black Hole. ApJ, 875(1):L1, Apr. 2019. doi: 10.3847/2041-8213/ab0ec7.

A. Fabian. Observational evidence of active galactic nuclei feedback. *Annual Review of Astronomy and Astrophysics*, 50:455–489, 2012.

B. L. Fanaroff and J. M. Riley. The morphology of extragalactic radio sources of high and low luminosity. *Monthly Notices of the Royal Astronomical Society*, 167 (1):31P–36P, 1974.

E. A. Fath. The spectra of some spiral nebulae and globular star clusters. *Publications of the Astronomical Society of the Pacific*, 21(126):138–143, 1909.

E. D. Feigelson, S. A. Laurent-Muehleisen, R. I. Kollgaard, and E. B. Fomalont. Discovery of Inverse-Compton X-Rays in Radio Lobes. ApJ, 449:L149, Aug. 1995. doi: 10.1086/309642.

E. Fermi. On the Origin of the Cosmic Radiation. *Physical Review*, 75(8):1169–1174, Apr. 1949. doi: 10.1103/PhysRev.75.1169.

L. Ferrarese and D. Merritt. A fundamental relation between supermassive black holes and their host galaxies. *The Astrophysical Journal Letters*, 539(1):L9, 2000.

W. A. Fowler and F. Hoyle. *Star formation.* HM Stationery Office, 1963.

J. Frank, A. King, D. Raine, et al. *Accretion power in astrophysics.* Cambridge university press, 2002.

K. Gebhardt, R. Bender, G. Bower, A. Dressler, S. Faber, A. V. Filippenko, R. Green, C. Grillmair, L. C. Ho, J. Kormendy, et al. A relationship between nuclear black hole mass and galaxy velocity dispersion. *The Astrophysical Journal Letters*, 539(1):L13, 2000.

M. Georganopoulos, J. Kirk, and A. Mastichiadis. The beaming pattern and spectrum of radiation from inverse compton scattering in blazars. *The Astrophysical Journal*, 561(1):111, 2001.

M. Georganopoulos, E. S. Perlman, D. Kazanas, and J. McEnery. Quasar x-ray jets: Gamma-ray diagnostics of the synchrotron and inverse compton hypotheses: The case of 3c 273. *The Astrophysical Journal Letters*, 653(1):L5, 2006.

A. M. Ghez, S. Salim, N. N. Weinberg, J. R. Lu, T. Do, J. K. Dunn, K. Matthews, M. R. Morris, S. Yelda, E. E. Becklin, T. Kremenek, M. Milosavljevic, and J. Naiman. Measuring Distance and Properties of the Milky Way's Central Supermassive Black Hole with Stellar Orbits. ApJ, 689(2):1044–1062, Dec. 2008. doi: 10.1086/592738.

H. E. S. S. Collaboration, H. Abdalla, R. Adam, F. Aharonian, F. Ait Benkhali, E. O. Angüner, M. Arakawa, C. Arcaro, C. Armand, H. Ashkar, M. Backes, V. Barbosa Martins, M. Barnard, Y. Becherini, D. Berge, K. Bernlöhr, R. Blackwell, M. Böttcher, C. Boisson, J. Bolmont, S. Bonnefoy, J. Bregeon, M. Breuhaus, F. Brun, P. Brun, M. Bryan, M. Büchele, T. Bulik, T. Bylund, M. Capasso, S. Caroff, A. Carosi, S. Casanova, M. Cerruti, T. Chand, S. Chandra, A. Chen, S. Colafrancesco, M. Curyło, I. D. Davids, C. Deil, J. Devin, P. deWilt, L. Dirson, A. Djannati-Ataï, A. Dmytriiev, A. Donath, V. Doroshenko, L. O. Drury, J. Dyks, K. Egberts, G. Emery, J. P. Ernenwein, S. Eschbach, K. Feijen, S. Fegan, A. Fiasson, G. Fontaine, S. Funk, M. Füßling, S. Gabici, Y. A. Gallant, F. Gaté, G. Giavitto, D. Glawion, J. F. Glicenstein, D. Gottschall, M. H. Grondin, J. Hahn, M. Haupt, G. Heinzelmann, G. Henri, G. Hermann, J. A. Hinton, W. Hofmann, C. Hoischen, T. L. Holch, M. Holler, D. Horns, D. Huber, H. Iwasaki, M. Jamrozy, D. Jankowsky, F. Jankowsky, A. Jardin-Blicq, I. Jung-Richardt, M. A. Kastendieck, K. Katarzyński, M. Katsuragawa, U. Katz, D. Khangulyan, B. Khélifi, J. King, S. Klepser, W. Kluźniak, N. Komin, K. Kosack, D. Kostunin, M. Kraus, G. Lamanna, J. Lau, A. Lemière, M. Lemoine-Goumard, J. P. Lenain, E. Leser, C. Levy, T. Lohse, I. Lypova, J. Mackey, J. Majumdar, D. Malyshev, V. Marandon, A. Marcowith, A. Mares, C. Mariaud, G. Martí-Devesa, R. Marx, G. Maurin, P. J. Meintjes, A. M. W. Mitchell, R. Moderski, M. Mohamed, L. Mohrmann, C. Moore, E. Moulin, J. Muller, T. Murach, S. Nakashima, M. de Naurois, H. Ndiyavala, F. Niederwanger, J. Niemiec, L. Oakes, P. O'Brien, H. Odaka, S. Ohm, E. de Ona Wilhelmi, M. Ostrowski, I. Oya, M. Panter, R. D. Parsons, C. Perennes, P. O. Petrucci, B. Peyaud, Q. Piel, S. Pita, V. Poireau, A. Priyana Noel, D. A. Prokhorov, H. Prokoph, G. Pühlhofer, M. Punch, A. Quirrenbach, S. Raab, R. Rauth, A. Reimer, O. Reimer, Q. Remy, M. Renaud, F. Rieger, L. Rinchiuso, C. Romoli, G. Rowell, B. Rudak, E. Ruiz-Velasco, V. Sahakian, S. Saito, D. A. Sanchez, A. Santangelo, M. Sasaki, R. Schlickeiser, F. Schüssler, A. Schulz, H. M. Schutte, U. Schwanke, S. Schwemmer, M. Seglar-Arroyo, M. Senniappan, A. S. Seyffert, N. Shafi, K. Shiningayamwe, R. Simoni, A. Sinha, H. Sol, A. Specovius, M. Spir-Jacob, Ł. Stawarz, R. Steenkamp, C. Stegmann, C. Steppa, T. Takahashi, T. Tavernier, A. M. Taylor, R. Terrier, D. Tiziani, M. Tluczykont, C. Trichard, M. Tsirou, N. Tsuji, R. Tuffs, Y. Uchiyama, D. J. van der Walt, C. van Eldik, C. van Rensburg, B. van Soelen, G. Vasileiadis, J. Veh, C. Venter, P. Vincent, J. Vink, F. Voisin, H. J. Völk, T. Vuillaume, Z. Wadiasingh, S. J.

Wagner, R. White, A. Wierzcholska, R. Yang, H. Yoneda, M. Zacharias, R. Zanin, A. A. Zdziarski, A. Zech, A. Ziegler, J. Zorn, and N. Żywucka. Resolving acceleration to very high energies along the jet of Centaurus A. Nature, 582(7812): 356–359, June 2020. doi: 10.1038/s41586-020-2354-1.

M. J. Hardcastle. Testing the beamed inverse-compton model for jet x-ray emission: velocity structure and deceleration. *Monthly Notices of the Royal Astronomical Society*, 366(4):1465–1474, 2006.

M. J. Hardcastle, M. Birkinshaw, and D. M. Worrall. Chandra observations of the X-ray jet in 3C 66B. *Monthly Notices of the Royal Astronomical Society*, 326(4): 1499–1507, Oct. 2001. doi: 10.1111/j.1365-2966.2001.04699.x.

M. J. Hardcastle, D. M. Worrall, R. P. Kraft, W. R. Forman, C. Jones, and S. S. Murray. Radio and x-ray observations of the jet in centaurus a. *The Astrophysical Journal*, 593(1):169–183, Aug 2003. ISSN 1538-4357. doi: 10.1086/376519. URL http://dx.doi.org/10.1086/376519.

D. Harris and H. Krawczynski. X-ray emission processes in radio jets. *The Astrophysical Journal*, 565(1):244, 2002.

D. Harris and H. Krawczynski. X-ray emission from extragalactic jets. *Annu. Rev. Astron. Astrophys.*, 44:463–506, 2006.

D. E. Harris and H. Krawczynski. Constraints on the Nature of Jets from KPC Scale X-Ray Data. In *Revista Mexicana de Astronomia y Astrofisica, vol. 27*, volume 27 of *Revista Mexicana de Astronomia y Astrofisica Conference Series*, page 188, Mar 2007.

J. J. Harwood, M. J. Hardcastle, and J. H. Croston. Spectral ageing in the lobes of cluster-centre fr ii radio galaxies. *Monthly Notices of the Royal Astronomical Society*, 454(4):3403–3422, Oct 2015. ISSN 1365-2966. doi: 10.1093/mnras/stv2194. URL http://dx.doi.org/10.1093/mnras/stv2194.

S. Heinz and M. C. Begelman. Jet acceleration by tangled magnetic fields. *The Astrophysical Journal*, 535(1):104, 2000.

W. Herschel. On the construction of the heavens. by william herschel, esq. f. r. s. *Philosophical Transactions of the Royal Society of London*, 75:213–266, 1785. ISSN 02610523. URL http://www.jstor.org/stable/106755.

B. S. Hogan, M. L. Lister, P. Kharb, H. L. Marshall, and N. J. Cooper. Chandra Discovery of 10 New X-ray Jets Associated with FR II Radio Core-selected AGNs in the MOJAVE Sample. ApJ, 730:92, Apr. 2011. doi: 10.1088/0004-637X/730/2/92.

D. Hogg, G. MacDonald, R. Conway, and C. Wade. Synthesis of brightness distribution in radio sources. *The Astronomical Journal*, 74:1206–1213, 1969.

E. Hubble. A relation between distance and radial velocity among extra-galactic nebulae. *Proceedings of the National Academy of Sciences*, 15(3):168–173, 1929.

W. Huggins. Xiii. on the spectra of some of the nebulœ. a supplement to the paper "on the spectra of some of the fixed stars. *Philosophical Transactions of the Royal Society of London*, (154):437–444, 1864.

S. F. Hönig. Redefining the torus: A unifying view of agns in the infrared and submillimeter. *The Astrophysical Journal*, 884(2):171, Oct 2019. ISSN 1538-4357. doi: 10.3847/1538-4357/ab4591. URL http://dx.doi.org/10.3847/1538-4357/ab4591.

Ž. Ivezić, K. Menou, G. R. Knapp, M. A. Strauss, R. H. Lupton, D. E. V. Berk, G. T. Richards, C. Tremonti, M. A. Weinstein, S. Anderson, et al. Optical and radio properties of extragalactic sources observed by the first survey and the sloan digital sky survey. *The Astronomical Journal*, 124(5):2364, 2002.

K. G. Jansky. Directional studies of atmospherics at high frequencies. *Proceedings of the Institute of Radio Engineers*, 20(12):1920–1932, 1932.

S. Jester, D. Harris, H. L. Marshall, and K. Meisenheimer. New chandra observations of the jet in 3c 273. i. softer x-ray than radio spectra and the x-ray emission mechanism. *The Astrophysical Journal*, 648(2):900, 2006.

I. Kant. *Allgemeine Naturgeschichte und Theorie des Himmels, oder Versuch von der Verfassung und dem mechanischen Ursprunge des ganzen Weltgebäudes: nach Newtonschen Grundsätzen abgehandelt*. 1755.

J. Kataoka, D. Harris, A. Siemiginowska, M. Ostrowski, M. Swain, M. Hardcastle, J. Goodger, K. Iwasawa, P. Edwards, et al. Chandra reveals twin x-ray jets in the powerful fr ii radio galaxy 3c 353. *The Astrophysical Journal*, 685(2):839, 2008.

K. Kellermann and I. Pauliny-Toth. The spectra of opaque radio sources. *The Astrophysical Journal*, 155:L71, 1969.

E. Y. Khachikian and D. W. Weedman. An atlas of seyfert galaxies. *The Astrophysical Journal*, 192:581–589, 1974.

P. Kharb, M. L. Lister, H. L. Marshall, and B. S. Hogan. Chandra and HST Imaging of the Quasars PKS B0106+013 and 3C 345: Inverse Compton X-Rays and Magnetized Jets. ApJ, 748(2):81, Apr. 2012. doi: 10.1088/0004-637X/748/2/81.

S. Komissarov and S. Falle. The large-scale structure of fr-ii radio sources. *Monthly Notices of the Royal Astronomical Society*, 297(4):1087–1108, 1998.

A. Konigl. *Relativistic effects in extragalactic radio sources*. California Institute of Technology, 1980.

R. A. Laing and A. Bridle. Adiabatic relativistic models for the jets in the radio galaxy 3c 31. *Monthly Notices of the Royal Astronomical Society*, 348(4):1459–1472, 2004.

M. L. Lister, M. F. Aller, H. D. Aller, M. A. Hodge, D. C. Homan, Y. Y. Kovalev, A. B. Pushkarev, and T. Savolainen. MOJAVE. XV. VLBA 15 GHz Total Intensity and Polarization Maps of 437 Parsec-scale AGN Jets from 1996 to 2017. ApJS, 234(1):12, Jan 2018. doi: 10.3847/1538-4365/aa9c44.

H. Liu, B. Luo, W. Brandt, M. S. Brotherton, S. Gallagher, Q. Ni, O. Shemmer, and J. Timlin. On the observational difference between the accretion disk–corona connections among super-and sub-eddington accreting active galactic nuclei. *The Astrophysical Journal*, 910(2):103, 2021.

M. S. Longair. *Synchrotron radiation*, page 193–227. Cambridge University Press, 3 edition, 2011. doi: 10.1017/CBO9780511778346.010.

D. Lynden-Bell. Galactic nuclei as collapsed old quasars. *Nature*, 223(5207):690–694, 1969.

J. Magorrian, S. Tremaine, D. Richstone, R. Bender, G. Bower, A. Dressler, S. Faber, K. Gebhardt, R. Green, C. Grillmair, et al. The demography of massive dark objects in galaxy centers. *The Astronomical Journal*, 115(6):2285, 1998.

H. L. Marshall, B. P. Miller, D. S. Davis, E. S. Perlman, M. Wise, C. R. Canizares, and D. E. Harris. A high-resolution x-ray image of the jet in m87. *The Astrophysical Journal*, 564(2):683–687, jan 2002. doi: 10.1086/324396. URL https://doi.org/10.1086%2F324396.

H. L. Marshall, D. Schwartz, J. Lovell, D. Murphy, D. Worrall, M. Birkinshaw, J. Gelbord, E. Perlman, and D. Jauncey. A chandra survey of quasar jets: first results. *The Astrophysical Journal Supplement Series*, 156(1):13, 2005.

H. L. Marshall, M. J. Hardcastle, M. Birkinshaw, J. Croston, D. Evans, H. Landt, E. Lenc, F. Massaro, E. S. Perlman, D. A. Schwartz, et al. A flare in the jet of pictor a. *The Astrophysical Journal Letters*, 714(2):L213, 2010.

H. L. Marshall, J. M. Gelbord, D. A. Schwartz, D. W. Murphy, J. E. J. Lovell, D. M. Worrall, M. Birkinshaw, E. S. Perlman, L. Godfrey, and D. L. Jauncey. An X-ray Imaging Survey of Quasar Jets: Testing the Inverse Compton Model. ApJS, 193(1):15, Mar. 2011. doi: 10.1088/0067-0049/193/1/15.

H. L. Marshall, J. M. Gelbord, D. M. Worrall, M. Birkinshaw, D. A. Schwartz, D. L. Jauncey, G. Griffiths, D. W. Murphy, J. E. Lovell, E. S. Perlman, et al. An x-ray imaging survey of quasar jets: the complete survey. *The Astrophysical Journal*, 856(1):66, 2018.

J.-M. Martí. Numerical simulations of jets from active galactic nuclei. *Galaxies*, 7 (1):24, 2019.

T. A. Matthews and A. R. Sandage. Optical Identification of 3C 48, 3C 196, and 3C 286 with Stellar Objects. ApJ, 138:30, July 1963. doi: 10.1086/147615.

J. E. McClintock, R. Narayan, and J. F. Steiner. Black hole spin via continuum fitting and the role of spin in powering transient jets. In *The Physics of Accretion onto Black Holes*, pages 295–322. Springer, 2013.

J. C. McKinney. General relativistic magnetohydrodynamic simulations of the jet formation and large-scale propagation from black hole accretion systems. *Monthly Notices of the Royal Astronomical Society*, 368(4):1561–1582, 2006.

A. L. McNamara, Z. Kuncic, and K. Wu. X-ray polarization in relativistic jets. *Monthly Notices of the Royal Astronomical Society*, 395(3):1507–1514, 2009.

D. L. Meier. The theory and simulation of relativistic jet formation: towards a unified model for micro-and macroquasars. *New Astronomy Reviews*, 47(6-7): 667–672, 2003.

E. T. Meyer, M. Georganopoulos, W. B. Sparks, L. Godfrey, J. E. Lovell, and E. Perlman. Ruling out ic/cmb x-rays in pks 0637-752 and the implications for tev emission from large-scale quasar jets. *The Astrophysical Journal*, 805(2):154, 2015.

E. T. Meyer, W. B. Sparks, M. Georganopoulos, J. Anderson, R. van der Marel, J. Biretta, S. T. Sohn, M. Chiaberge, E. Perlman, and C. Norman. An hst proper-motion study of the large-scale jet of 3c273. *The Astrophysical Journal*, 818(2): 195, 2016.

E. T. Meyer, M. Petropoulou, M. Georganopoulos, M. Chiaberge, P. Breiding, and W. B. Sparks. Detection of an optical/uv jet/counterjet and multiple spectral components in m84. *The Astrophysical Journal*, 860(1):9, 2018.

E. T. Meyer, A. R. Iyer, K. Reddy, M. Georganopoulos, P. Breiding, and M. Keenan. The origin of the x-ray emission in two well-aligned extragalactic jets: The case for IC/CMB. *The Astrophysical Journal*, 883(1):L2, sep 2019. doi: 10.3847/2041-8213/ab3db3. URL https://doi.org/10.3847%2F2041-8213%2Fab3db3.

B. P. Miller, W. N. Brandt, S. Gallagher, A. Laor, B. J. Wills, G. Garmire, and D. P. Schneider. X-ray absorption and an x-ray jet in the radio-loud broad absorption-line quasar pg 1004+ 130. *The Astrophysical Journal*, 652(1):163, 2006.

L. Mullin and M. Hardcastle. Bayesian inference of jet bulk-flow speeds in fanaroff–riley type ii radio sources. *Monthly Notices of the Royal Astronomical Society*, 398(4):1989–2004, 2009.

K. J. E. Northover. The radio galaxy 3C 66. MNRAS, 165:369, Jan 1973. doi: 10.1093/mnras/165.4.369.

M. S. S. L. Oei, R. J. van Weeren, M. J. Hardcastle, A. Botteon, T. W. Shimwell, P. Dabhade, A. R. D. J. G. I. B. Gast, H. J. A. Röttgering, M. Brüggen, C. Tasse, W. L. Williams, and A. Shulevski. The discovery of a radio galaxy of at least 5 Mpc. *arXiv e-prints*, art. arXiv:2202.05427, Feb. 2022.

J. Oke. Absolute energy distribution in the optical spectrum of 3c 273. *Nature*, 197 (4872):1040–1041, 1963.

E. Opik. An estimate of the distance of the andromeda nebula. *The Astrophysical Journal*, 55, 1922.

M. Ostrowski et al. Radiation from the relativistic jet: a role of the shear boundary layer. *The Astrophysical Journal*, 578(2):763, 2002.

F. Owen and M. Ledlow. The fri/il break and the bivariate luminosity function in abell clusters of galaxies. In *The Physics of Active Galaxies*, volume 54, page 319, 1994.

P. Padovani. The faint radio sky: radio astronomy becomes mainstream. *The Astronomy and Astrophysics Review*, 24(1), Sep 2016. ISSN 1432-0754. doi: 10.1007/s00159-016-0098-6. URL http://dx.doi.org/10.1007/s00159-016-0098-6.

P. Padovani. On the two main classes of active galactic nuclei. *Nature Astronomy*, 1(8), Jul 2017. ISSN 2397-3366. doi: 10.1038/s41550-017-0194. URL http://dx.doi.org/10.1038/s41550-017-0194.

B. Peterson. The broad-line region in active galactic nuclei. In *Physics of Active Galactic Nuclei at all Scales*, pages 77–100. Springer, 2006.

B. M. Peterson and K. Horne. Echo mapping of active galactic nuclei. *Astronomische Nachrichten*, 325(3):248–251, Mar 2004. ISSN 1521-3994. doi: 10.1002/asna.200310207. URL http://dx.doi.org/10.1002/asna.200310207.

M. Petropoulou, G. Vasilopoulos, and D. Giannios. The tev emission of ap librae: a hadronic interpretation and prospects for cta. *Monthly Notices of the Royal Astronomical Society*, 464(2):2213–2222, 2017.

C. Pfrommer, P. Chang, and A. E. Broderick. The cosmological impact of luminous tev blazars. iii. implications for galaxy clusters and the formation of dwarf galaxies. *The Astrophysical Journal*, 752(1):24, 2012.

S. Raimundo and A. Fabian. Eddington ratio and accretion efficiency in active galactic nuclei evolution. *Monthly Notices of the Royal Astronomical Society*, 396 (3):1217–1221, 2009.

G. Reber. Cosmic static. *Proceedings of the IRE*, 28(2):68–70, 1940.

K. Reddy, M. Georganopoulos, and E. T. Meyer. X-Ray-to-radio Offset Inference from Low-count X-Ray Jets. ApJS, 253(2):37, Apr. 2021. doi: 10.3847/1538-4365/abd8d7.

M. Rees, M. Begelman, R. Blandford, and E. Phinney. Ion-supported tori and the origin of radio jets. *Nature*, 295(5844):17–21, 1982.

C. Reynolds and A. Fabian. Rosat pspc observations of cygnus a: X-ray spectra of the cooling flow and hotspots. *Monthly Notices of the Royal Astronomical Society*, 278(2):479–487, 1996.

D. Richstone, E. Ajhar, R. Bender, G. Bower, A. Dressler, S. Faber, A. Filippenko, K. Gebhardt, R. Green, L. Ho, et al. Supermassive black holes and the evolution of galaxies. *nature*, 395(6701):A14–A19, 1998.

E. Salpeter. Accretion of interstellar matter by massive objects. *Publications*, 1:165, 1964.

R. M. Sambruna, J. K. Gambill, L. Maraschi, F. Tavecchio, R. Cerutti, C. Cheung, C. M. Urry, and G. Chartas. A survey of extended radio jets with chandra and the hubble space telescope. *The Astrophysical Journal*, 608(2):698, 2004.

R. M. Sambruna, M. Gliozzi, F. Tavecchio, L. Maraschi, and L. Foschini. The jet-disk connection in agns: Chandra and xmm-newton observations of three powerful radio-loud quasars. *The Astrophysical Journal*, 652(1):146, 2006.

M. Schmidt. 3c 273: a star-like object with large red-shift. *Nature*, 197(4872): 1040–1040, 1963.

E. J. Schreier, P. Gorenstein, and E. D. Feigelson. High-resolution x-ray observations of m87-nucleus, jet and radio halo. *The Astrophysical Journal*, 261:42–50, 1982.

D. Schwartz, H. Marshall, J. Lovell, B. Piner, S. Tingay, M. Birkinshaw, G. Chartas, M. Elvis, E. Feigelson, K. Ghosh, et al. Chandra discovery of a 100 kiloparsec x-ray jet in pks 0637–752. *The Astrophysical Journal Letters*, 540(2):L69, 2000.

C. K. Seyfert. Nuclear emission in spiral nebulae. *The Astrophysical Journal*, 97: 28, 1943.

N. I. Shakura and R. A. Sunyaev. Reprint of 1973A&A....24..337S. Black holes in binary systems. Observational appearance. A&A, 500:33–51, June 1973.

H. Shapley and H. D. Curtis. The Scale of the Universe. *Bulletin of the National Research Council*, 2(11):171–217, May 1921.

A. Siemiginowska, Ł. Stawarz, C. Cheung, D. Harris, M. Sikora, T. L. Aldcroft, and J. Bechtold. The 300 kpc long x-ray jet in pks 1127–145, z= 1.18 quasar: Constraining x-ray emission models. *The Astrophysical Journal*, 657(1):145, 2007.

M. Sikora and G. Madejski. On pair content and variability of subparsec jets in quasars. *The Astrophysical Journal*, 534(1):109, 2000.

M. Sikora, M. C. Begelman, G. M. Madejski, and J.-P. Lasota. Are quasar jets dominated by poynting flux? *The Astrophysical Journal*, 625(1):72, 2005.

A. K. Singal. Maximum brightness temperature of an incoherent synchrotron source: Inverse compton limit—a misnomer. *The Astrophysical Journal*, 703(2):L109, 2009.

V. M. Slipher. The radial velocity of the andromeda nebula. *Lowell Observatory Bulletin*, 2:56–57, 1913.

Ł. Stawarz, M. Sikora, M. Ostrowski, and M. C. Begelman. On multiwavelength emission of large-scale quasar jets. *The Astrophysical Journal*, 608(1):95, 2004.

M. R. Swain, A. H. Bridle, and S. A. Baum. Internal structure of the jets in 3c 353. *The Astrophysical Journal Letters*, 507(1):L29, 1998.

F. Tavecchio, L. Maraschi, R. M. Sambruna, and C. M. Urry. The x-ray jet of pks 0637–752: Inverse compton radiation from the cosmic microwave background? *The Astrophysical Journal Letters*, 544(1):L23, 2000.

F. Tavecchio, G. Ghisellini, and A. Celotti. Clumps in large scale relativistic jets. *Astronomy & Astrophysics*, 403(1):83–91, 2003.

A. Tchekhovskoy, R. Narayan, and J. C. McKinney. Efficient generation of jets from magnetically arrested accretion on a rapidly spinning black hole. *Monthly Notices of the Royal Astronomical Society: Letters*, 418(1):L79–L83, 2011.

B. D. Turland. 3c 219: A double radio source with a jet. *Monthly Notices of the Royal Astronomical Society*, 172(1):181–189, 1975.

Y. Uchiyama. Emission from large-scale jets in quasars. *International Journal of Modern Physics D*, 17(09):1475–1481, Sep 2008. ISSN 1793-6594. doi: 10.1142/s0218271808013054. URL http://dx.doi.org/10.1142/S0218271808013054.

Y. Uchiyama, C. M. Urry, P. Coppi, J. Van Duyne, C. Cheung, R. M. Sambruna, T. Takahashi, F. Tavecchio, and L. Maraschi. An infrared study of the large-scale jet in quasar pks 1136–135. *The Astrophysical Journal*, 661(2):719, 2007.

C. M. Urry and P. Padovani. Unified schemes for radio-loud active galactic nuclei. *Publications of the Astronomical Society of the Pacific*, 107(715):803, 1995.

J.-M. Wang, P. Du, C. Hu, H. Netzer, J.-M. Bai, K.-X. Lu, S. Kaspi, J. Qiu, Y.-R. Li, F. Wang, and SEAMBH Collaboration. Supermassive Black Holes with High Accretion Rates in Active Galactic Nuclei. II. The Most Luminous Standard Candles in the Universe. ApJ, 793(2):108, Oct. 2014. doi: 10.1088/0004-637X/793/2/108.

J. Wardle and S. Aaron. How fast are the large-scale jets in quasars? constraints on both doppler beaming and intrinsic asymmetries. *Monthly Notices of the Royal Astronomical Society*, 286(2):425–435, 1997.

A. R. Whitney, I. I. Shapiro, A. E. Rogers, D. S. Robertson, C. A. Knight, T. A. Clark, R. M. Goldstein, G. E. Marandino, and N. R. Vandenberg. Quasars revisited: rapid time variations observed via very-long-baseline interferometry. *Science*, 173(3993):225–230, 1971.

C. J. Willott, S. Rawlings, K. M. Blundell, and M. Lacy. The emission line—radio correlation for radio sources using the 7c redshift survey. *Monthly Notices of the Royal Astronomical Society*, 309(4):1017–1033, 1999.

L. Woltjer. A magnetostatic model for a compressible star. *The Astrophysical Journal*, 131:227, 1960.

D. Worrall. The x-ray jets of active galaxies. *The Astronomy and Astrophysics Review*, 17(1):1–46, 2009.

D. M. Worrall and M. Birkinshaw. X-ray synchrotron emission from the oblique shock in the jet of the powerful radio galaxy 3C346. MNRAS, 360:926–934, July 2005. doi: 10.1111/j.1365-2966.2005.09082.x.

T. Wright. *An Original Theory Or New Hypothesis of the Universo, Founded Upon the Laws of Nature, and Solving by Mathematical Principles the General Phaenomena of the Visible Creation and Particularly the Via Lactea*. Chapelle, 1750. URL https://books.google.com/books?id=80VZAAAAcAAJ.

Y. B. Zel'dovich and I. D. Novikov. Estimating the mass of a super-star. In *Doklady Akademii Nauk*, volume 158, pages 811–814. Russian Academy of Sciences, 1964.